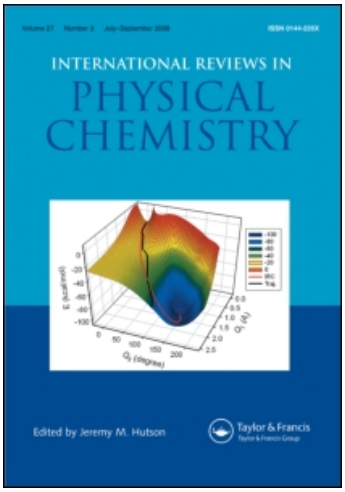

International Reviews in Physical Chemistry
Publication details, including instructions for authors and subscription information:
http://www.informaworld.com/smpp/title~content=t713724383

Fifth-order two-dimensional Raman spectroscopy: A new direct probe of the liquid state

Kevin J. Kubarych[a]; Chris J. Milne[a]; R. J. Dwayne Miller[a]
[a] Departments of Chemistry and Physics, University of Toronto, Toronto, Ontario, Canada

Online publication date: 26 November 2010

To cite this Article Kubarych, Kevin J. , Milne, Chris J. and Miller, R. J. Dwayne(2003) 'Fifth-order two-dimensional Raman spectroscopy: A new direct probe of the liquid state', International Reviews in Physical Chemistry, 22: 3, 497 — 532
To link to this Article: DOI: 10.1080/0144235031000121544
URL: http://dx.doi.org/10.1080/0144235031000121544

INT. REVIEWS IN PHYSICAL CHEMISTRY, 2003
VOL. 22, NO. 3, 497–532

Taylor & Francis
Taylor & Francis Group

Fifth-order two-dimensional Raman spectroscopy: a new direct probe of the liquid state

KEVIN J. KUBARYCH, CHRIS J. MILNE and R. J. DWAYNE MILLER*

Departments of Chemistry and Physics, University of Toronto, Toronto, Ontario M5S 1H6, Canada

The experimental challenges of performing high-order non-linear spectroscopies have been met using diffractive optics to allow passive phase locking of all six interacting laser fields and true phase-sensitive detection. Improvements in signal to noise, use of phase contrast, as well as geometrical phase matching and polarization have made it possible to isolate systematically the pure nuclear fifth-order Raman response. Using CS_2 as a model system of a simple liquid, the two-time correlation of the probed liquid modes or bath memory function is found to decay faster than the free-induction decay associated with one-dimensional spectroscopic probes of the same modes. This observation is in sharp contrast to other two-dimensional spectroscopies and is related to the unique application of a two-quantum transition or Raman overtone for the rephasing pathway. Both theory and experiment have converged on this point, as well as a pronounced ridge along the probe time axis that is related to population decay of the excited modes. Recent advances in theoretical treatments of the correlation function have shown this spectroscopy to contain a wealth of information imbedded in the specific form of the two-dimensional spectrum. The extremely sensitive nature of this experiment stems from the involvement of a Raman overtone that gives the experiment direct access to the all important anharmonic terms in the intermolecular potential. As such, this form of spectroscopy harbours great promise to provide a rigorous benchmark for developing liquid state theories. The experimental details, current state of understanding of the experiment, interpretation and pitfalls, as well as an overview of the various theoretical efforts are given. The area is at a critical cross-road in advancing the spectroscopy to other liquids and associated complex systems. Some speculations on what the future holds are given in this context. The onus is clearly on experimentalists to advance this method and new technologies will be needed to do so—in which directly probing the dynamical structure of liquid water is the ultimate challenge.

Contents

*Author to whom correspondence should be addressed. E-mail: dmiller@lphys.chem.utoronto.ca

International Reviews in Physical Chemistry ISSN 0144–235X print/ISSN 1366–591X online © 2003 Taylor & Francis Ltd
http://www.tandf.co.uk/journals
DOI: 10.1080/0144235031000121544

1. Introduction

The formulation of a complete microscopic picture of chemical processes ultimately requires an understanding of solution phase dynamics. Although an elaborate architecture of theory and experiment has been successfully developed to treat chemical reactions in the gas phase, the medium in which most molecular transformations occur—from the mundane to the spectacular—is in solution. Indeed, the significance of liquid water is so overwhelming that the search for extraterrestrial life is tantamount to establishing the presence of water on distant worlds [1]. It is, therefore, in the interest of obtaining a detailed understanding of liquid dynamics that considerable effort has been applied to the refinement of multidimensional spectroscopies to provide new experimental observables of the liquid state [2–49]. Just over a half-century has passed since the first coherent multidimensional spectroscopy measurement was reported [50] and it is now evident that many spectroscopic techniques can derive qualitative benefits from higher dimensionality owing to the direct connection to high-order correlation functions of the liquid. Although recent progress in multidimensional electronic and infrared (IR) spectroscopies has advanced vigorously, this review will focus instead on multidimensional Raman spectroscopy as a probe of ultrafast liquid dynamics. Although there are some important differences between the three main spectroscopic regions, the general principles of multidimensional approaches are nevertheless universal. In other words, lessons learned in multidimensional Raman spectroscopy offer insights into IR and electronic techniques. To justify the emphasis on high-order Raman processes, a brief description of the information content of the alternatives with respect to probing the liquid state is given below.

There have been two paths taken in the development of ultrafast probes of liquid or solution dynamics. One avenue has been to observe the influence of the liquid bath dynamics *indirectly* by studying the electronic response of a probe molecule in solution [51–58]. The alternative route has been to probe the bath *directly* by accessing the low-frequency intermolecular modes through third-order electronically non-resonant Raman interactions [59–63]. Both of these lines of attack, while inherently useful, are not capable of determining the total liquid response at a level suitable for a detailed description. The study of solvent–solute systems has been addressed in the past using dynamic Stokes shift and photon echo measurements, as well as various other transient techniques [64]. Since the timescale on which a solvent modifies the electronic structure of a solute is intrinsically fast, these techniques are examples of ultrafast, time-resolved spectroscopies where one ideally attempts to have a time resolution that is faster than a typical molecular vibrational period (i.e. several tens of femtoseconds). It should be noted that, although quantum mechanics relates the energy spectrum directly to the dynamics, the spectra of condensed phase systems are significantly broadened by various mechanisms, and the only recourse is to use non-linear optical methods in the time domain. One important example of time-domain non-linear spectroscopy is the photon echo [54]. By observing the rephasing ability of a reporter solute molecule, it is possible to characterize the time-dependent effect of the surrounding solvent molecules or bath on the solute's electronic structure. Using a variant on the stimulated photon echo, for example, the basic principles of polar solvation have essentially been fully resolved temporally and the observables have been found to provide complementary information to other approaches [64–66].

Solute–solvent dynamics are certainly crucial to developing a deeper appreciation of condensed phase reaction dynamics. Electronically resonant echo-based experiments rely on very robust and well-characterized probe dye molecules which can be chosen to absorb strongly at a convenient wavelength for ultrafast laser excitation. However, the ability to extract information about the liquid alone from such measurements is complicated by the fact that the signal contains a convolution of solvent and solute dynamics in addition to any coupling. The main difficulty in applying resonant echo spectroscopy to the study of bulk liquid dynamics stems from the fact that the reporter chromophore is not a small perturbation on the liquid structure and may itself have non-trivial intramolecular dynamics. Furthermore, electronically resonant echoes essentially probe the solute–solvent coupling that is intimately connected to excited electronic states that are potentially irrelevant to ground state reaction dynamics. Additionally, the solute–solvent coupling cannot be connected to the dynamics of the liquid without assumptions about the solute perturbation to the local liquid structure. Despite this unavoidable entanglement of the solute–solvent dynamics, resonant echo-based approaches have provided valuable insight into many photochemical reactions and are becoming widely adopted in a number of diverse settings including the binding of antibodies to receptors [67].

On the other hand, a list of powerful, non-resonant optical techniques have emerged that provide a direct probe of the liquid dynamics without the need for a solute. The principal methods of studying low-frequency motions are optical Kerr effect (OKE) spectroscopy [59, 60, 68–71] coherent anti-Stokes Raman scattering [72–74], coherent Stokes Raman scattering [75, 76], Raman-induced Kerr effect spectroscopy [60, 77–79], and others. Each of these is a member of a general class of non-linear optical processes called '*four-wave mixing*'. The generated signals are produced by an induced polarization that is a product of three external electric fields and the material's third-order non-linear susceptibility; hence these measurements are all referred to as '*third-order*' processes. We would like to emphasize right at that outset that measurements of this genre are not multidimensional despite the non-linear interaction and use of multiple fields. Rather, these experimental methods depend only on a single variable—either a single delay time or a single frequency—and as such are examples of *one-dimensional* (1D) spectroscopies that can be rigorously connected to linear frequency domain analogues [80, 81]. In contrast, measurements that depend on any two variables (i.e. two time delays, two frequencies or one of each) are said to be '*two dimensional*'. As they are typically implemented, time domain electronically non-resonant third-order spectroscopies have a single time delay, and the decay in the observed signal reflects the spectral width of the initially prepared vibrational transitions. Non-resonant third-order measurements provide valuable insight into the differences in dynamics attributable to isotropic and anisotropic motions [82], but unfortunately they are insensitive to anharmonicity in the intermolecular potential and the relative contributions of different line broadening mechanisms [81]. Non-resonant third-order spectroscopy provides a straightforward projection of the low-frequency spectrum of a liquid, but is incapable of further subdividing that spectrum in order to recover the underlying line shapes or dynamical anharmonicity.

The limitations of 1D processes—those involving only a single time or frequency variable—are not technical shortcomings, but rather are consequences of a fundamental Fourier transform relationship between the 1D time-domain observable

and the absorption spectrum (i.e. the 1D frequency-domain measurement) [81]. With respect to directly probing the solvent coordinate, the alternative would be to use the equivalent to the resonant photon echo discussed above but at wavelengths tuned to low-frequency motions of the liquid state. In this case, the frequencies of the excitation pulses have to lie within 0–500 cm^{-1}, corresponding to the intermolecular spectrum of motions for most liquids. This excitation wavelength range corresponds to THz frequencies. Despite rapid progress in this area, the sources for THz spectroscopies are not sufficiently intense to conduct such non-linear studies. In fact, at the time of writing, there has not been a non-linear THz experiment successfully demonstrated, although numerous groups are attempting such studies.

The only real choice at present is to rely on Raman excitation processes to address directly the low-frequency spectrum of the liquid state. Current laser source technology is well advanced to provide sufficient peak power to drive non-linear Raman interactions along with ultrashort pulse durations to give a real-time view of the motions. The challenge is to develop sufficiently sensitive experimental methods to enable isolation of the desired Raman process while separating this signal component from a plethora of other high-order field interactions that invariably begin to contribute at the high powers needed to observe stimulated Raman scattering. Theoretical connections of the Raman field interactions to the microscopic details are also needed. In this regard, Tanimura and Mukamel made a seminal contribution by discovering a rephasing pathway for the induced Raman polarization that involved only six fields, rather than the eight field interactions that would be required for a Raman process to be rigorously equivalent to resonant third-order echo-based spectroscopies [2]. The rephasing pathway that cancels inhomogeneous broadening involves a Raman overtone or two-quantum transition. With further refinements in experiment and theory, we have learned that the direct connection to the anharmonic terms in the intermolecular potential through the involvement of a Raman overtone makes this method exquisitely sensitive to the details of the intermolecular potential. This new spectroscopy may well develop to be the most definitive probe of liquids. Strictly speaking, each Raman interaction requires two fields. In an echo-based pulse protocol, the use of an initial excitation step, a rephasing step, and a probe of the net induced polarization, must involve at least six fields to lowest order for an all-Raman process, one of which is the signal field. Consequently, there are five external fields which combine, via the fifth-order non-linear susceptibility, to generate the sixth field (or signal). Two-dimensional Raman is, therefore, an example of *six-wave mixing* and is a *fifth-order* process. Fifth-order Raman is the lowest-order electronically non-resonant technique capable of distinguishing between inhomogeneous and homogeneous line broadening. This fact provides simplification in the total number of field interactions and directly connects the observable to the anharmonic terms in the intermolecular potential—two key features that make this method a truly powerful new probe of liquids.

2. Theoretical background

Drawing on the important conclusions regarding the limits of one-dimensional response functions by Loring and Mukamel [80, 81], the theory underlying fifth-order Raman spectroscopy was initially developed by Tanimura and Mukamel using an analytical approach that made it possible to discern the key rephasing pathways within a total of 32 possible time-domain terms [2]. This astute observation has

led to several advances in the theoretical underpinnings that have shown that the fifth-order Raman response is particularly sensitive to mode–mode couplings [12, 14, 41, 83, 84], vibrational anharmonicity [6, 8, 15, 46, 85–92], vibrational level-dependent dephasing processes and population relaxation [12, 14, 43]. The fifth-order response was treated using multimode Brownian oscillator (MMBO) models [2, 31, 84, 93] as well as instantaneous normal modes analysis [5, 15, 20, 92]. More recently, coupled-mode theory has been employed to generate the fifth-order response of an atomic liquid [16, 17, 94–96] while direct molecular dynamics (MD) simulations have been carried out for both atomic and molecular liquids [6, 15, 21, 22, 97–100]. This section describes the basic formulation of the fifth-order response function and some simple harmonic models to illustrate the sensitivity to the underlying dynamics.

The fifth-order Raman pulse sequence involves a series of three Raman interactions separated by two independent time delays. Figure 1 shows some common representations of the field interactions. At the time origin, two fields, E_1 and E_2, with wavevectors $\mathbf{k}_1$ and $\mathbf{k}_2$ drive a Raman coherence. After a time delay, τ_2, two fields, E_3 and E_4, with wavevectors $\mathbf{k}_3$ and $\mathbf{k}_4$ transfer the first coherence to a new coherence. After a second time delay, τ_4, a probe field, E_5, with wavevector $\mathbf{k}_5$ interrogates the net induced polarization and generates a fifth-order phase-matched signal, E_s, with wavevector $\mathbf{k}_s = (\mathbf{k}_1 - \mathbf{k}_2) - (\mathbf{k}_3 - \mathbf{k}_4) + \mathbf{k}_5$. Figure 1 (*b*) shows an energy level diagram representation of this series of field interactions. This type of diagram, however, is very limited in its ability to describe the full richness of the multiple pathways by which the density matrix can be manipulated by the interacting

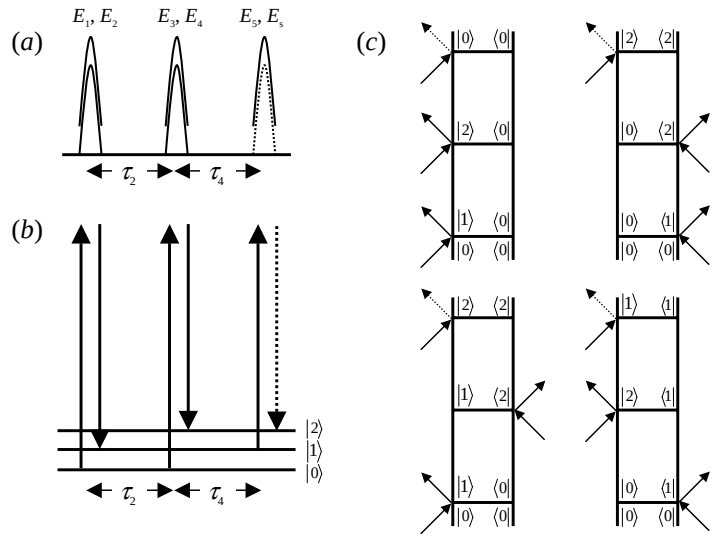

Figure 1. Several diagrams indicating the fifth-order Raman pulse sequence. (*a*) Pulses with fields E_1 and E_2 interacting at $t = 0$, followed by two pulses at $t = \tau_2$ with fields E_3 and E_4, and at $t = \tau_2 + \tau_4$ the probe field, E_5, generates a signal E_s. (*b*) Energy level diagram showing one possible Liouville space pathway. (*c*) Four double-sided Feynman diagrams that contribute to the two-dimensional response—time proceeds in the vertical direction with the ket side of the density matrix represented by the left vertical line, and the bra is represented by the right vertical line, and arrows pointed towards (away from) the vertical lines indicate absorption (emission).

fields. A more complete picture of high-order non-linear spectroscopies can be seen in a double-sided Feynman diagram [101]. There are eight Liouville space pathways for the case when τ_2 and τ_4 are greater than zero, and four of these are shown in figure 1(*c*) (the other four are complex conjugates of the four shown). Double-sided Feynman diagrams are better able to depict the fact that the bra and ket sides of the density matrix can be manipulated separately by the interacting fields [102]. As is discussed below, the experimentally observable fifth-order Raman response function is directly related to tracking the evolution of the density matrix along different Liouville space pathways.

The derivation of the non-linear response functions that determine all non-linear spectroscopy methods proceeds according to a straightforward argument. The density matrix is expanded in powers of the applied electric field, and, using the interaction picture expression for the propagator in Liouville space, an expression is obtained for the *N*th-order term of the time-dependent density matrix, $\rho^{(N)}(t)$. For an electronically non-resonant Raman interaction, the total Hamiltonian is broken up into two parts [102]:

$$H(t) = H_0 - \alpha E(t)^2 \tag{1}$$

where H_0 denotes the field-free ('system') part, α is the polarizability operator and $E(t)$ is the electric field. The emitted signal field, $E_s(t)$, is proportional to the polarization which is, by definition, the expectation value of the dipole operator using the time-evolved density matrix. Tanimura and Mukamel showed that the fifth-order polarization is given by

$$P^{(5)}(\mathbf{r}, t) = \int_0^\infty \mathrm{d}\tau_4 \int_0^\infty \mathrm{d}\tau_2 E(\mathbf{r}, t)\left|E(\mathbf{r}, t-\tau_2)\right|^2 \left|E(\mathbf{r}, t-\tau_2-\tau_4)\right|^2 R^{(5)}(\tau_2, \tau_4), \tag{2}$$

where

$$R^{(5)}(\tau_2,\tau_4) = \left(\frac{i}{\hbar}\right)^2 \left\langle \left\{[\alpha(\tau_2+\tau_4),\alpha(\tau_2)],\alpha(0)\right\}\rho_{\mathrm{eq}}\right\rangle \tag{3}$$

is the fifth-order response function and ρ_{eq} is the initial equilibrium density matrix [2]. It is the response function that is of principal interest since, under the conventional delta-function pulse assumption (impulsive limit) and the slowly varying envelope approximation, the generated signal field is directly proportional to the response function itself. The signal field, $E_s(t)$, due to the induced fifth-order polarization over a path length, L, is given by [103]

$$E_s(t) = 2\pi i \frac{\omega_s^2}{k_s c^2} \int_0^L \mathrm{d}z\, P^{(5)}(z,t)\, \mathrm{e}^{i\,\Delta k\, z} \tag{4}$$

where ω_s is the signal field radial frequency, k_s is the signal wavevector, c is the speed of light, and Δk is the wavevector mismatch for generation of the signal. In the impulsive limit, the integral can be rewritten as

$$E_s(\tau_2,\tau_4) \propto i \frac{\omega_s}{n_s} \int_0^L \mathrm{d}z\, E_1 E_2 E_3 E_4 E_5 R^{(5)}(\tau_2,\tau_4)\, \mathrm{e}^{i\,\Delta k\, z} \tag{5}$$

where n_s is the index of refraction at the signal wavelength and the expression for the polarization, equation (2), has been used. The integration over the propagation coordinate, z, is straightforwardly evaluated and yields

$$E_s(\tau_2,\tau_4) = i\frac{L\omega_s}{n_s}E^5 R^{(5)}(\tau_2,\tau_4)\frac{\sin(\Delta k\, L/2)}{\Delta k\, L/2}\exp(i\,\Delta k\, L/2) \tag{6}$$

where the simplifying assumption that $E_1E_2E_3E_4E_5 = E^5$ has been made.

The signal field is composed of several different parts, including some that are experimentally adjustable parameters. The path length, frequency, field strength and wavevector mismatch can all be chosen within the constraints of current femtosecond laser technology. The signal field, equation (6), has been derived without including the transverse extent (x and y dependence) of the interacting laser fields, and thus is a plane wave result. In real experiments the laser beams are Gaussian fields, and this difference can be taken into account, but efforts to do so have revealed few significant consequences for the generated signal field [42, 43]. The most important observations to make about the signal field are (1) it depends linearly on the path length, (2) it is proportional to the response function and (3) it has an overall phase and amplitude that are functions of the wavevector mismatch and sample path length.

Theoretical treatments of the material properties that give rise to the two-dimensional fifth-order Raman observable are concerned primarily with developing a model system for which the fifth-order response, $R^{(5)}(\tau_2, \tau_4)$, can be evaluated. The simplest conceivable model for nuclear dynamics is a harmonic oscillator. By considering a single harmonic oscillator, ignoring for the moment any coupling to an environment, it is possible to illustrate two key differences between fifth-order and third-order Raman spectroscopy. The response function of equation (3) is a three-point time correlation function of the polarizability operator, and the many-body polarizability operator generally depends on all the nuclear coordinates of the system. Considering only a single harmonic mode, q_j, we can expand the polarizability operator about some equilibrium displacement, q_0, in a Taylor series as [12, 20, 104].

$$\alpha(q_j) = \alpha(q_0) + \left[\frac{\partial\alpha(q_j)}{\partial q_j}\right]_{q_0} q_j + \left[\frac{\partial^2\alpha(q_j)}{\partial q_j^2}\right]_{q_0} q_j^2 + \cdots. \tag{7}$$

By identifying the nth partial derivative with respect to the coordinate as $\alpha^{(n)}$, the expansion can be rewritten as

$$\alpha(q_j) = \alpha^{(0)} + \alpha^{(1)}q_j + \alpha^{(2)}q_j^2 + \cdots. \tag{8}$$

In the case of multiple modes, it should be kept in mind that the polarizability is mode dependent. The zeroth-order term does not contribute to the response since it does not depend on the coordinate and is therefore time independent. The first non-zero contribution is proportional to the linear displacement of the coordinate, and it is this term that is responsible for typical third-order Raman processes. For the harmonic model considered here, the linear polarizability leads to coherences between states that differ by one quantum number ($\Delta n = \pm 1$). The fact that $\alpha^{(1)}$ generates one-quantum coherences can easily be verified by evaluating the matrix element of the q_j operator using the harmonic basis.

In figures 1(*b*) and (*c*), each pair of arrows represents one operation with the polarizability, and in principle only consideration of the full polarizability is exact. The expansion of equation (8) is useful, however, in determining what types of coherences can be involved in the fifth-order Raman response. If each interaction occurs via an $\alpha^{(1)}$ process, regardless of the initial state, the signal will vanish identically with zero trace (which is equivalent to saying that the final density matrix is in a coherence). The pathway that results in a population density matrix using the lowest order of interactions is $\alpha^{(2)}\alpha^{(1)}\alpha^{(1)}$, where the second-order interaction can occur at any of the three time points. In other words, within the single harmonic mode model, generation of a signal requires a two-quantum coherence to be created by one of the interactions. Since the $\alpha^{(2)}$ term in the polarizability depends on the square of the displacement, it is known as the '*non-linear polarizability*'.

The requirement for a non-linearity in the polarizability is simply due to the condition that the final density matrix must be in a population (diagonal) and that the linear polarizability can only create one-quantum coherences such as $|n\rangle\langle n+1|$ or $|n+1\rangle\langle n|$ (where the states $|n\rangle$ are eigenstates of the harmonic mode q_j). Should the states deviate from harmonicity, the selection rules would be lifted and the requirement for non-linear polarizability is likewise relaxed. Therefore one can imagine at least two scenarios where anharmonicity is responsible for the fifth-order response. Either the anharmonicity can be a fundamental property of the nuclear mode as in the case for typical intramolecular vibrational modes, or the anharmonicity may be due to the time-evolving potential surface where the frequency of the otherwise harmonic mode changes in time. The latter situation has been denoted '*dynamical anharmonicity*' in order to emphasize the key distinction that the 'system' Hamiltonian (H_0 in equation (1)) is not, in fact, time independent [92]. While there is no doubt that the true potential surface of a liquid is anharmonic, it is nevertheless instructive to retain some sort of modal description as long as possible in order to take advantage of our intuition of harmonic systems.

To summarize the above discussion, from considerations based on a harmonic model, it is evident that the fifth-order Raman signal requires at minimum either non-linear polarizability or vibrational anharmonicity [2]. There is one remaining interaction that must be addressed in order to complete the list of possible pathways in a fifth-order measurement. By extending the model from one with only a single harmonic mode to one that considers at least two modes (q_1 and q_2), the polarizability (equation (7)) can be rewritten as

$$\alpha(q_1,q_2) = \alpha^{(0)} + \sum_{j=1,2} \alpha_j^{(1)} q_j + \sum_{j,k=1,2} \alpha_{jk}^{(2)} q_j q_k + \cdots \tag{9}$$

where the polarizability is expanded about an equilibrium configuration, $\mathbf{q}_0$, and

$$\alpha_{jk}^{(2)} = \left[\frac{\partial\alpha(q_1,q_2)}{\partial q_j \partial q_k}\right]_{\mathbf{q}_0}. \tag{10}$$

In equation (9), the linear term is simply the sum of the linear polarizability of each mode, while the non-linear term gains the ability to couple orthogonal modes. For the case where $j=k$, the non-linear term reflects the non-linear polarizability of the two individual modes, but, when $j\neq k$, the two modes can be coupled solely through the polarizability (i.e. the Hamiltonian is still fully harmonic and the two modes are uncoupled). This so-called '*mode-mixing through polarizability*' has been investigated

by Saito and Ohmine, and Steffen and Duppen [5, 12, 14, 41, 83, 84]. The ability to generate combination band coherences also makes it possible to investigate couplings between high-frequency intramolecular Raman-active modes. While one experimental effort did attempt to measure intramolecular coupling, the experimental results were complicated by lower-order artifacts [41].

The preceding discussion concentrated on the details of signal generation by emphasizing the importance of non-linear polarizability, vibrational anharmonicity and mode mixing through the polarizability. In order to appreciate the full richness of fifth-order Raman spectroscopy, some attention must be paid to a model of relaxation processes that can be determined by this new experimental measurement. In the common parlance of condensed phase spectroscopy—where spectral signatures are generally broad and featureless—two limits have been constructed in order to explain the origins of the broadening. Whatever the technique, spectroscopy determines the energy level gap between at least two states, and the fluctuations of the energy gap are directly related to a decay of a time-dependent signal or the width of a frequency-domain spectrum. In the limit of very high frequency variations in the energy gap due to rapid collisions with the surrounding solvent molecules, the transition is said to be homogeneously broadened. At the other extreme, static variations due to locally distinct configurations (sometimes called 'sites') naturally give rise to an inhomogeneous distribution of energy gaps that generally lacks dynamical information. In a liquid, however, there are clearly no truly static 'sites' since the molecules must be free to diffuse, and collisions can very rapidly force a given local configuration to evolve even on short timescales. Yet there are very clear signs that in hydrogen-bonded liquids, for example, the strong intermolecular interactions lead to persistent structured arrangements of water molecules that can last over reasonably long (~ps) timescales [105, 106]. The long-lived configurations, therefore, suggest that key dynamical properties of liquids such as water can be separated into liquid-like disorder with very fast fluctuations and slowly interconverting structured transients. It has been a challenge to both theory and experiment over several years to develop spectroscopic methods capable of distinguishing between these two limiting classifications, and, for the low-frequency motions of liquids, fifth-order Raman is the lowest-order electronically non-resonant approach [2, 81].

A very physical approach to the modelling of the non-linear optical response of a system coupled to a bath was developed by Mukamel and co-workers, and has come to be known as the MMBO method [102]. MMBO treats the system as a set of harmonic oscillators that are coupled to a harmonic heat bath. Each system mode is characterized by a frequency, a dephasing rate (or line width) and a coupling strength (or weighting factor), and these oscillators may correspond to actual localized vibrational modes or to generalized coordinates. Tanimura and Mukamel showed that the *n*th-order non-linear response function can be evaluated using this method of parametrization [2]. Shortly after the initial proposal of fifth-order Raman, Palese *et al.* [31] employed an MMBO approach in order to simulate the fifth-order response of liquid water in the homogeneous and inhomogeneous limits. The spectral density of water was determined by parametrizing the third-order response as measured by a time-domain optical heterodyne detected (OHD) optical Kerr effect measurement [60]. A parametrization using six Brownian oscillators was found to reproduce faithfully, the spectral density, thus providing the six sets of frequencies, widths and weights needed to evaluate any non-linear response function.

The fifth-order response of liquid water, simulated using the MMBO parametrization, is shown in figure 2 for the case of purely homogeneous broadening (figure 2(*a*)) and inhomogeneous broadening (figure 2(*b*)). It is clear from these simulations that the fifth-order response is highly sensitive to the degree of inhomogeneous broadening, as evidenced by the dramatic echo-like feature along the time diagonal ($\tau_1 = \tau_2$). Since the third-order response is identical for the two broadening cases, this study illustrates the inherent richness of the higher-order correlation function responsible for the signal in a fifth-order Raman experiment. In analogy to resonant electronic and spin multipulse experiments, this diagonal feature has become known as a vibrational or motional 'echo', as it is a direct consequence of the inhomogeneous broadening in the system. Although there are several reasons to be sceptical of the response functions shown in figure 2, they do illustrate one of the chief advantages of fifth-order Raman over lower-order techniques: within a harmonic picture, even considering a structured spectral density such as that of liquid water, there is considerable ability to discern different contributions to the line shape. The rephasing process involves not just a single transition as in conventional echo-based third-order spectroscopies but a distribution of distinctly different types of motions. In the case of water, the distinct classes of motions consist of the librational components involving different combinations of the three different moments of inertia for water (200–1000 cm^{-1}), translational acoustic-like displacements of the central pentamer hydrogen-bonded structure (180 cm^{-1}), transverse displacements or shearing-type motions (60 cm^{-1})

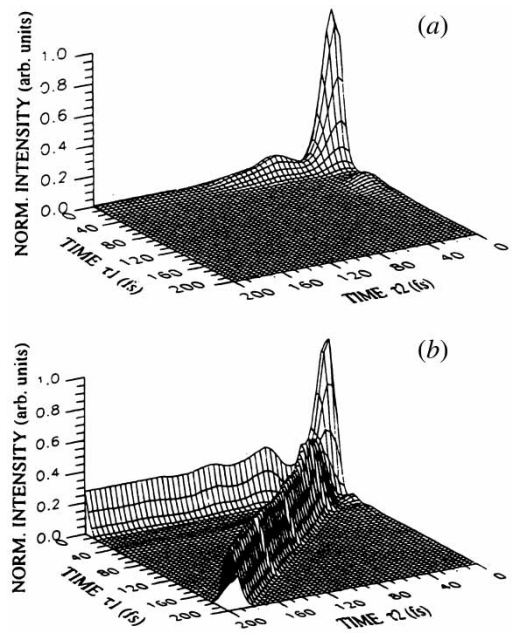

Figure 2. Simulated fifth-order Raman response of liquid water using the MMBO model with six Brownian oscillators parameterized with a fit to the OHD-OKE response: (*a*) purely homogeneous case; (*b*) purely inhomogeneous case. The pronounced echo signature along the time diagonal, $\tau_1 = \tau_2$, is indicative of inhomogeneous broadening. Reproduced with permission from *J. Phys. Chem.*, 1994, **98**, 12466–12470. Copyright 1994 American Chemical Society.

and diffusive reorientational motions ($< 100\ cm^{-1}$). It is important to note that even with this set of effectively different oscillators the fifth-order response is capable of distinguishing inhomogeneous from homogenous contributions. The observable projects out the two time-interval correlation or memory function of the bath and provides an inclusive response with little interference between different modes in the response function, and, where present, the signature of mode mixing or anharmonic coupling between modes is evident.

The MMBO model for dynamics in the presence of a bath (or more generally any *dissipation*) is a strategy that has been broadly applied to many diverse areas of physics, and, as such, it is not a microscopic description of the liquid. There are several possibilities for microscopic treatments of the nuclear dynamics including exact quantum mechanics, exact classical dynamics and various approximations such as instantaneous normal modes [15, 92, 107–109], quenched normal modes [5] and mode-coupling theory [16, 17, 94–96]. A fully quantum mechanical treatment of real liquids is impossible at present and is likely to remain so for many years. On the other hand, exact classical MD simulations are tenable and have been carried out for liquid xenon and liquid carbon disulphide and water in order to evaluate the fifth-order response [6, 15, 21, 22, 97–99]. These microscopically based approaches will be discussed in section 4.

The fifth-order Raman response offers a qualitatively superior probe of the dynamics of liquids by being able, in principle, to report directly on the degree of inhomogeneous broadening in a system. This section has examined some features of the fifth-order response within the framework of a harmonic picture of the liquid modes in order to build on a relatively well-developed intuition for harmonic motion. The results of experiments and simulations, however, strongly indicate that such a simplified picture is at best incomplete and may in fact be beyond repair. In order to analyse the results of microscopic treatments and actual experiments, however, the harmonic picture is a good starting point. The next section will present an overview of the experimental implementation of fifth-order Raman spectroscopy while considering the response of liquid CS_2.

3. Experimental advances

As much as it has challenged the theoretical community, the fifth-order Raman response has been particularly difficult to isolate in the laboratory. It is generally true that non-linear optical processes become increasingly weaker as the order of non-linearity increases, and in the case of fifth-order Raman spectroscopy this is compounded by the potential requirement for non-linearity in the polarizability. In addition to the intrinsically weak non-linear signal, there are cascaded third-order processes that can be collinear with the direct fifth-order signal and must be removed in order to access the rich information content promised by the fifth-order response [48, 110–112]. Furthermore, the cascaded third-order signals have incident laser power dependences that are identical to the desired fifth-order signal and are thus not separable through power dependence measurements. Several strategies have been followed in order to attempt to minimize the contribution of third-order cascades to the measured signal. By combining several approaches including a diffractive optic beam splitter, optical heterodyne detection (OHD), two- and three-colour pulse sequences and an appropriately thin sample path length, we have made substantial progress in isolating the fifth-order Raman response of liquid CS_2 [45–49].

The fifth-order Raman pulse sequence (figure 1) produces a signal field with wavevector $\mathbf{k}_s = (\mathbf{k}_1 - \mathbf{k}_2) - (\mathbf{k}_3 - \mathbf{k}_4) + \mathbf{k}_5$ and there is considerable freedom in selecting an experimental beam geometry where the wavevector mismatch, $\Delta\mathbf{k}$, for the direct fifth-order signal can be made to be very small. The wavevector mismatch is a critical value inasmuch as it determines the overall optical signal amplitude (cf. equation (6)), and, in the case of multiple signal components, the amplitude and phase of each component depend on its degree of wavevector mismatch. As can be seen in equation (6), the wavevector mismatch is not the only determinant of the amplitude or phase of a signal since the path length is similarly important, and this will be discussed below.

Assuming that a proper beam geometry is found that satisfies wavevector matching for the direct fifth-order signal, one must then determine the degree of wavevector matching for the third-order cascades by considering the individual intermediate steps [112]. Figure 3 shows energy level diagrams indicating the third-order cascade processes. There are two different types of cascading lower-order processes. The first of these, shown in figure 3 (*a*), was initially noted by Ivanecky and Wright, and has been denoted the 'sequential cascade' [110]. The sequential cascade is composed of two different third-order interactions that take place on different sets of molecules, where the signal generated in the first step acts as a pump field in the second step (indicated by broken lines). There are two different sequential pathways corresponding to two different combinations of wavevectors that lead to

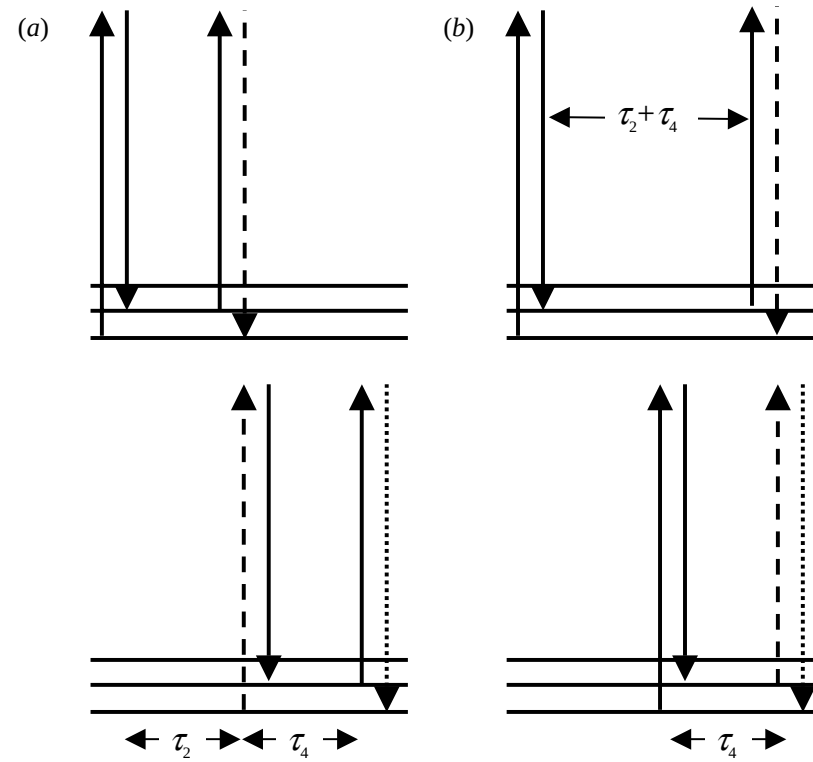

Figure 3. Energy level diagrams showing the (*a*) sequential and (*b*) parallel cascaded third-order processes. The broken lines indicate intermediate fields, and the dotted lines are final signal fields.

signals in the same direction as the direct fifth-order process. Figure 3(*b*) shows another kind of cascade, detailed by Blank *et al.* [112], where two simultaneous third-order processes conspire to generate a signal in the fifth-order direction when the signal of one third-order intermediate acts as a probe in the other. There are similarly two different pathways for the so-called 'parallel cascade'. In all, there are a total of four distinct cascaded third-order signal pathways, and each one is expected to be orders of magnitude larger in intrinsic amplitude than the desired direct fifth-order signal [112].

Unfortunately, only the sequential cascade was known when the initial experimental results were reported. The first fifth-order Raman experiments of room temperature CS_2 were reported by Tominaga and Yoshihara [32–35, 88, 113–118], and these were followed by Steffen and Duppen [13, 36, 37, 119] and Tokmakoff and Fleming [39–41, 120]. Although all of these experiments were conducted with different laser sources and beam geometries, the results seemed to show reasonably good agreement. The experimental results did not, however, produce signals that were in accord with general theoretical predictions. The dominant feature of the measured data was a pronounced ridge along the pump pair delay axis (τ_2 in the convention adopted here), while the signals were found to decay very rapidly along the probe delay axis (τ_4). Nearly all theoretical analyses of the fifth-order response show that the signal along the τ_2 axis (when $\tau_4 = 0$) should vanish. Several theoretical attempts were made to explain this form of the response, and it appeared as though mode mixing through polarizability produced the most successful agreement [13]. It was ultimately demonstrated, however, that the data were due to parallel cascaded third-order processes that had been neglected in the design of the experimental beam geometries [112]. To give some insight into the difficulty in discerning the true nuclear fifth-order response, the form of the response function derived by Steffen and Duppen for mode-mixing through polarizability is identical to the cascaded third-order response functions found by Blank *et al.* Assignments cannot be made solely on the grounds of calculated response functions with various built-in assumptions but need to be checked experimentally to be free of cascade contributions using different beam geometries and other contrast mechanisms.

With the ultimate goal of measuring the fifth-order response of other liquids such as hydrogen-bonded systems, we developed an alternative technique for implementing non-linear spectroscopy based on diffractive optical elements [45, 121–124]. The diffractive optic approach has many advantages over conventional beam splitters. Since any multibeam non-linear interaction can be thought of as diffraction from a grating, it is natural to imagine using a diffractive element to split the beams since the beam splitter is ultimately related to the non-linear process in the sample. In four-wave mixing experiments (i.e. third-order spectroscopy), for example, there are three popular beam geometries: a square or rectangular box, a line (two-colour case) or an equilateral triangle. Non-resonant third-order Raman spectroscopy involves two beams crossed at an angle that write a phase grating in the material from which a time-delayed probe pulse can diffract into the wavevector-matched direction, $\mathbf{k}_s = (\mathbf{k}_1 - \mathbf{k}_2) + \mathbf{k}_3$. By designing a diffractive optic to generate the necessary beam pattern, implementation of four- (and six-)wave mixing experiments has been shown to be greatly simplified since there is no ambiguity in signal alignment [122]. Furthermore, in instances where there is added information in repeating an experiment under different grating wavevector conditions, a single optic with multiple diffraction gratings can be used where the time required to change the

grating wavevector (or 'fringe spacing') is reduced to the order of minutes [125]. Both diffusive processes and photoacoustics depend on the grating wavevector, and using a multiple-grating optic has been found to be very convenient. For the six-wave mixing geometries used in fifth-order Raman spectroscopy, because of the highly sensitive nature of the wave vector matching on signal phases and amplitudes, one ideally would prefer to have the beam pattern predetermined to prevent adjustments from latching onto poorer geometric phase matching that enhances the lower-order cascades. The diffractive optic approach provides this important constraint.

In addition to the strict constraints on beam geometry, a diffractive optic approach also enables the use of OHD by acting as a phase reference for what is fundamentally an interferometric measurement [122]. The experimental configuration is shown schematically in figure 4 for our most recent three-colour variation of this experiment and is the most general case. The pulses needed for the fifth-order Raman experiment are created by passing three time-delayed input pulses through the diffractive optic, where each pulse is diffracted according to the spatially periodic phase profile of the optic. We only require two beams from each of these patterns, and this is accomplished by introducing a slight tilt between the three input beams and blocking diffracted beams that are not needed. The end result is three pairs of pulses, two of which are used for the pump pairs, and the third is the probe–local oscillator pair. The local oscillator is a beam that is designed into the diffractive optic such that it is collinear with the generated signal beam. The relative intensity of this local oscillator was also designed into the optic so that it serves the dual purpose of aiding in detector alignment while acting as a reference field needed for OHD at near optimal amplitudes for the experimental conditions. The only phases relevant to the ultimate signal field phase are those between pulses within a given pair, and these phases are determined at the instant of diffraction. All the diffracted beams are imaged to the sample using two off-axis parabolic mirrors that are common to all six beams. This feature of the diffractive optic approach is the most important as it ensures that there are no independent paths for any of the beams. The diffractive optic serves as a phase reference and all beam pairs are generated at that point. The phase noise from various sources (primarily thermally induced pathlength variations) imparted on the beam propagation after the diffractive optic is correlated for all beams. The largest remaining phase noise source is due to variations in air density over the small distance between beams and this can be effectively handled with beam tubes and enclosures. Thus, the phase instability of uncorrelated independent optical paths common to beam-splitter-based interferometers is completely avoided. The passive phase stability of the diffractive optic apparatus for third-order Raman experiments was measured to be $\sim\lambda/300$ [122], and we estimate the phase stability for the fifth-order set-up to be at the $\lambda/50$ level over a period of a few hours. The only way to achieve this level of phase stability with conventional beam-splitter interferometers is by using active feedback requiring a reference interferometer for *each of the three pulse pairs*.

The advantages of OHD of non-linear signals are becoming broadly appreciated in multidimensional electronic and vibrational IR and Raman spectroscopy [27, 28, 79, 126–131]. Heterodyne detection linearizes the experimental observable while allowing the direct observations of any sign changes. Many Fourier transform techniques require that one has measured a signal proportional to the response

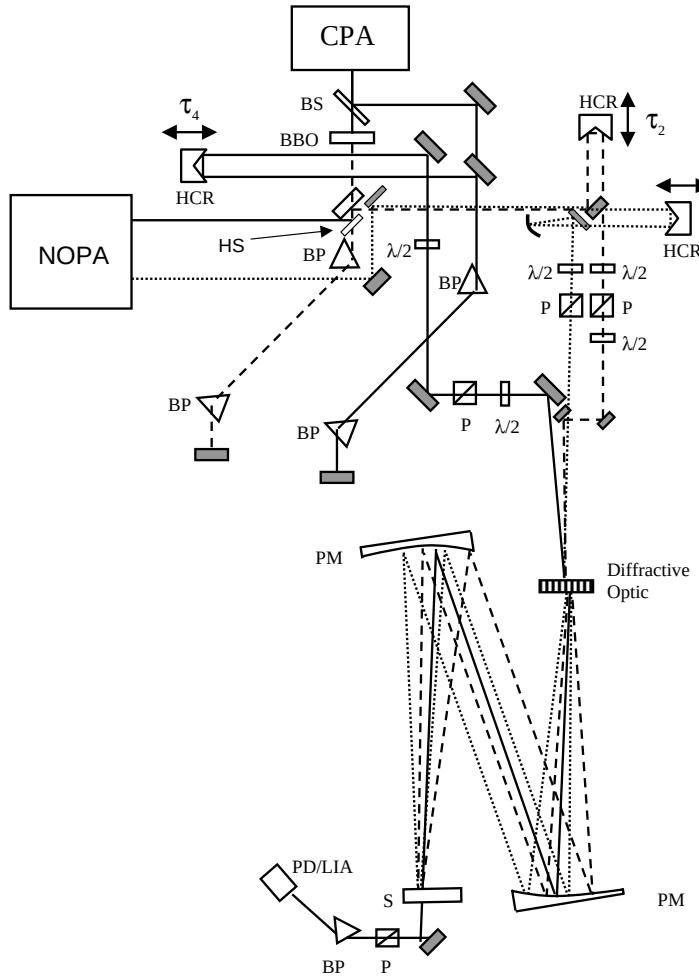

Figure 4. Experimental diagram for the most general three-colour case. HS, harmonic separator; BS, beam splitter; BBO, β-barium borate crystal; HCR, hollow cube retroreflector; BP, Brewster prism; CS, cover slip; λ/2, half-wave plate; P, polarizer; PM, parabolic mirror; S, sample; PD/LIA, photodiode–lock-in amplifier. The full lines indicate 800 nm beams, the dotted lines are the 530 nm beams and the broken lines are the 400 nm beams.

function itself rather than the squared modulus of the response since it is necessary to be able to assign the real and imaginary parts of the signal. Direct detected (or '*homodyne detection*' in the conventional jargon of ultrafast spectroscopy) signals are proportional to the square of the response function and are thus inappropriate for use with Fourier transform methods or deconvolution procedures without imposing significant assumptions. Since the heterodyne-detected observable is proportional to the amplitude of the signal field, the power dependence of the measured signal is reduced by a square root. The six-wave mixing signal intensity is proportional to the product of the five interacting laser pulse intensities, and thus the signal has an I^5 power dependence, while the heterodyne-detected signal has an E^5 dependence. Heterodyne detection also allows significant amplification of the non-linear signal through the necessary mixing with a reference local oscillator

whose amplitude can be set to be very large. There are limits to the degree of amplification that is possible [126], but, since these limits are due mainly to laser stability and background scatter level, improved laser technology and careful filtering can be expected to alleviate most of the limitations. Finally, heterodyne detection is a phase-sensitive measurement technique and in complicated multi-component signals, such as those containing more than one signal field contribution, it is possible to select one signal component out of several competing signals by appropriately adjusting the relative optical phase between the local oscillator and signal fields. As will be shown below, there is a relative phase difference between the cascaded third-order signals and the direct fifth-order signal, thus allowing the phase-sensitive features of heterodyne detection to be used as an additional contrast agent against the parasitic lower-order contaminants.

On a square-law photodetector, the time-domain interference between a signal field, $E_{\mathrm{sig}}(t)$, and reference field, $E_{\mathrm{ref}}(t)$, is given by [126]

$$\begin{aligned} I_{\mathrm{het}}(t) &= \left|E_{\mathrm{sig}}(t) + E_{\mathrm{ref}}(t)\right|^2 \\ &= \left|E_{\mathrm{sig}}(t)\right|^2 + \left|E_{\mathrm{ref}}(t)\right|^2 + 2E_{\mathrm{sig}}(t)E_{\mathrm{ref}}(t)\cos\Delta\phi \end{aligned} \tag{11}$$

where $\Delta\phi$ is the phase difference between the signal and reference fields and is given by

$$\Delta\phi = \phi_{\mathrm{ref}} - \left[\phi_\chi + \phi_{\mathrm{pr}} + \left(\phi_{\mathrm{pump1}} - \phi_{\mathrm{pump2}}\right) + \left(\phi_{\mathrm{pump3}} - \phi_{\mathrm{pump4}}\right)\right] \tag{12}$$

where ϕ_{ref} is the reference phase, ϕ_χ is any phase shift due to the material response, ϕ_{pr} is the probe phase and the remaining phases are those of the pump fields. Equation (12) indicates that the relative phases of the pulses within each of the three pairs determine the overall signal phase. For a successful implementation of heterodyne detection, it is necessary to keep the phases constant over the course of any measurement, and this task is more easily accomplished using the diffractive optic method as compared with active feedback of all three pulse pairs.

The heterodyne signal shown in equation (11) has two additional terms that are due to the direct detected signal and reference intensities. In order to recover the phase-sensitive term alone, it is necessary to remove the phase-insensitive direct detected terms. In the implementation described here, elimination of the direct detected terms is accomplished by recording three sets of data: one with the reference and probe unblocked (heterodyne measurement), one with the reference blocked and one with the probe blocked. The two direct detected signals are then subtracted from the heterodyne signal leaving only the phase-sensitive part. It is also possible to remove the phase-insensitive components by recording only two signals, where there is a π phase shift between the signals [128]. This *phase cycling* approach is a common technique in multidimensional nuclear magnetic resonance spectroscopy where is it very easy to impose arbitrary phase shifts with high precision. In the optical regime, however, where the wavelength of light is truly microscopic, errors in setting the phase can seriously complicate the signal processing.

The fifth-order Raman signal is detected using lock-in amplification where a single pump beam is chopped, and a photodiode detects the signal. Since the reference beam travels through the interaction volume, it is always possible that the intensity of the reference beam itself is modulated by the pump pulses, thus leading to a chopped signal that can be recorded by the lock-in amplifier. It is therefore necessary to remove the reference modulation, and this is accomplished by

subtraction of the signal with the probe beam blocked. The signal due to the modulated reference resembles the OKE response of the system and is thus easily identified [46, 48].

In order to appreciate the phase contrast against lower-order processes afforded by heterodyne detection, it is necessary to consider the cascade signal field. By using the same approach as was used to obtain equation (6) for the direct fifth-order signal field, it is possible to show that the cascaded signal is given by [48]

$$E_{\mathrm{cas}}(\tau_2,\tau_4) = L^2 \frac{\omega_{\mathrm{cas}}}{n_{\mathrm{cas}}} \frac{\omega_{\mathrm{int}}}{n_{\mathrm{int}}} E^5 R^{(3)}_{\mathrm{cas}}(\tau_2,\tau_4)\, \mathrm{sinc}\left(\frac{\Delta k_a L}{2}\right) \mathrm{e}^{i(\Delta k_a L/2)}\, \mathrm{sinc}\left(\frac{\Delta k_b L}{2}\right) \mathrm{e}^{i(\Delta k_b L/2)} \tag{13}$$

where L is the path length, ω_{cas} and n_{cas} are the cascaded signal frequency and index of refraction, ω_{int} and n_{int} are the intermediate signal frequency and index of refraction, E is the field amplitude, $R^{(3)}_{\mathrm{cas}}(\tau_2,\tau_4)$ is the cascaded third-order response, Δk_a and Δk_b are the wavevector mismatch values for the first and second intermediate third-order steps and $\mathrm{sinc}(x)$ is $\sin(x)/x$. Comparison of equations (6) and (13) suggests that there are, in fact, key differences between the fifth-order and third-order signals despite the identical power dependence and near-collinear signal wavevectors. The cascaded signal depends on the square of the path length, while the direct fifth-order signal depends linearly on the path length [112]. Moreover, since the direct fifth-order signal is multiplied by an extra factor of i, there is a nominal $\pi/2$ phase shift between the two signals (assuming that all wavevector mismatch values are zero and that the response functions, $R^{(3)}_{\mathrm{cas}}$ and $R^{(5)}$ are real functions). The two exponential terms also determine the resulting signal phase relative to the direct signal, and, since the general strategy to reduce the cascade contribution is to impose a large wavevector mismatch for the intermediate third-order processes by the choice of beam geometry, the phase of the signal field will strongly depend on the path length. Typical values of the wavevector mismatch used in the fifth-order Raman experiments are in the range 50–1000 cm^{-1}, and path lengths from 0.1 mm to 1.0 mm have been used [42, 48].

It is worthwhile to discuss one final point regarding the use of optical heterodyne detection in order to measure the direct fifth-order Raman response while suppressing the unwanted cascaded third-order signals. The large wavevector mismatch for the intermediate steps of the third-order cascades necessarily leads to a phase shift of the cascaded signal relative to the direct signal. In principle it is possible to separate any two phase-shifted signals regardless of the relative phase shift between them, but, when the phase shift is not $\pi/2$, it is much more challenging to separate the signals and there is a penalty in signal amplitude. It is also desirable to ensure that the entire cascaded third-order signal has a single phase—if there is a phase shift between two pathways, say between one parallel pathway and one of the sequential pathways, the desired fifth-order signal will need to be separated from both cascaded signals. We have shown that using our crossed-beam geometry, the phase shift between the direct fifth-order signal and the cascades is, in fact, nearly $\pi/2$, thus avoiding the pitfalls addressed here.

Two beam geometries used to measure the six-wave mixing signal of CS_2 using the diffractive optic base heterodyne method are shown in figure 5. Once a particular phase matching geometry is chosen, it is then a straightforward procedure to Fourier transform this pattern to the corresponding diffractive optic. The most important

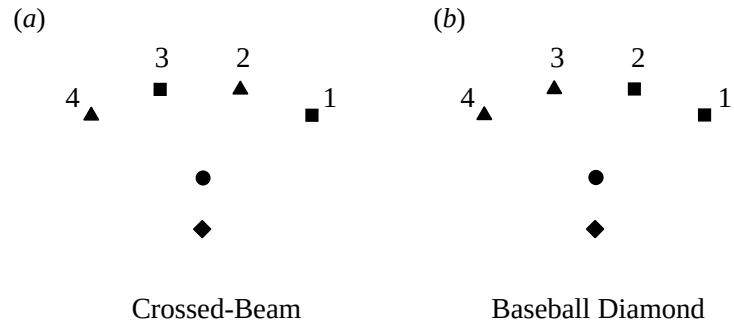

Figure 5. Two different experimentally implemented phase-matching beam geometries: (*a*) crossed beam and (*b*) baseball diamond. The crossed-beam geometry increases suppression of the cascaded third-order signals by a factor of 10 over the baseball diamond geometry.

detail is balancing the amplitude of the different Fourier components in the optic to give as broad a bandwidth as possible to be compatible with femtosecond pulses. The above patterns involved balancing 20 different Fourier components that gave a fairly flat wavelength dependence over the entire visible spectrum with up to 70% transfer efficiency to the target beam pattern [45]. With respect to figure 5, the only difference between these two beam geometries is their degree of wavevector mismatch for the parallel cascaded processes. The magnitude of the wavevector mismatch for the parallel cascade in the crossed-beam geometry is 10 times larger than it is in the baseball diamond geometry [45, 46]. The true power of the diffractive optic approach is illustrated by the relative ease with which it is possible to switch between the two beam geometries without realigning the signal, thus enabling a direct comparison of signals with varying degrees of contrast against lower-order cascades—an important experimental check on signal purity.

Another attractive feature of diffractive optics is that beams with different wavelengths will naturally be spatially separated owing to dispersion. In fact, single-colour experiments using diffractive optics are actually more challenging since it is necessary to introduce a slight angle between the incoming beams incident on the diffractive optic. In a non-resonant experiment, the optical wavelength is assumed to have no effect on the measured response, and one is therefore free to use different wavelengths for the pump and probe pulses. For the fifth-order Raman case, we adopted a two-colour approach where the pump pulses are the second harmonic of the 800 nm fundamental, and the probe and signal are the fundamental itself. There are several advantages in using a two-colour pulse sequence. Blue light interacts more strongly with the polarizability than does red light, leading to an expected increase (2^4) in the fifth-order signal relative to all 800 nm interaction for each Raman process [132]. Furthermore, since the pump and signal wavelengths are different, it is possible to prevent scattered pump light from reaching the detector by using spectral filtering via a prism. For small-angle beam geometries, scattered pump light is a common complication to signal detection. The final major advantage of using two colours for the pump and probe pulses is the suppression of coherent artifacts. In a single time variable experiment, one typically observes a large signal at the time origin owing to pulse width limited electronic hyperpolarizability. In a two-dimensional experiment, the electronic hyperpolarizability can be large enough in amplitude to mask smaller signal components well away from the time origin.

Additionally, the signal along the axes can be composed of combined electronic and nuclear hyperpolarizabilities, thus further obscuring any interesting direct nuclear dynamics [12]. From theoretical considerations, there is no nuclear contribution to the pure nuclear fifth-order signal along the τ_2 axis ($\tau_4 \sim 0$), but, along the τ_4 axis, there is an important contribution due to population relaxation. The use of two colours reduces the hyperpolarizability along the τ_2 axis and allows an estimate of the magnitude of the contribution along the τ_4 axis. In order to have a quantitative accounting of the electronic/nuclear hyperpolarizability along τ_4, however, a third wavelength needs to be used in one of the pump pairs [49].

The pioneering early reports of the fifth-order Raman response of liquid CS_2 represent, in all respects, landmark achievements in non-linear spectroscopy of liquids. They were, however, marred by the unfortunate coincidence of lower-order cascaded third-order signals. It is, therefore, the main goal of experimentalists to devise a strategy for separating the direct fifth-order Raman response from these competing processes. There have been several approaches [42, 44, 45, 128], and the one we have adopted is the multicolour diffractive optic based implementation combining OHD with a beam geometry that has large wavevector mismatch for the lower-order processes. In order to establish fifth-order Raman spectroscopy as a general methodology for studying condensed phase systems, it is necessary to demonstrate success in isolating the direct signal free of artifacts using a variety of contrast mechanisms to distinguish lower-order cascades from the nuclear fifth-order response of interest.

4. Case study: fifth-order response of liquid CS_2

Carbon disulphide has long been the subject of electronically non-resonant non-linear spectroscopy of liquids owing to its exceptionally large polarizability. Like most simple liquids, CS_2 has an essentially featureless Raman spectrum below $200\,cm^{-1}$, thus making it an ideal test bed for the experimental advances outlined above. The dominant intermolecular forces in CS_2 are due to van der Waals interactions, suggesting that the liquid may lack significant local structure relative to a strongly hydrogen-bonded network such as that in water. It should be a straightforward task, therefore, to recognize qualitative differences in the fifth-order Raman response for liquids at the two extremes.

We begin the discussion of the fifth-order Raman response of liquid CS_2 by considering the first reports following the realization that the previous experimental results had been dominated by lower-order artifacts. The two-colour diffractive optics based method was used with a 1 kHz amplified Ti:sapphire laser system. At this early stage, only the direct detected signal was reported, and the sample path length of 300 μm was larger than the subsequently used 100 μm path length [45]. The two-dimensional homodyne detected response of liquid CS_2 is shown in figure 6. Figure 6 (*c*) and (*d*) show the data obtained using the baseball diamond phase matching geometry, and figure 6 (*a*) and (*b*) show the results using the crossed-beam geometry. There is a dramatic difference between the two data sets punctuated by the disappearance of the nuclear signal contribution for positive and negative τ_2 time delays for the crossed beam geometry. The negative τ_2 time delay corresponds, in the case of a symmetric fifth-order tensor element, to a skewed image of the positive τ_2 delay response. The polarization configuration for the data shown in figure 6 is not formally a single tensor element. The four pump pulses are polarized

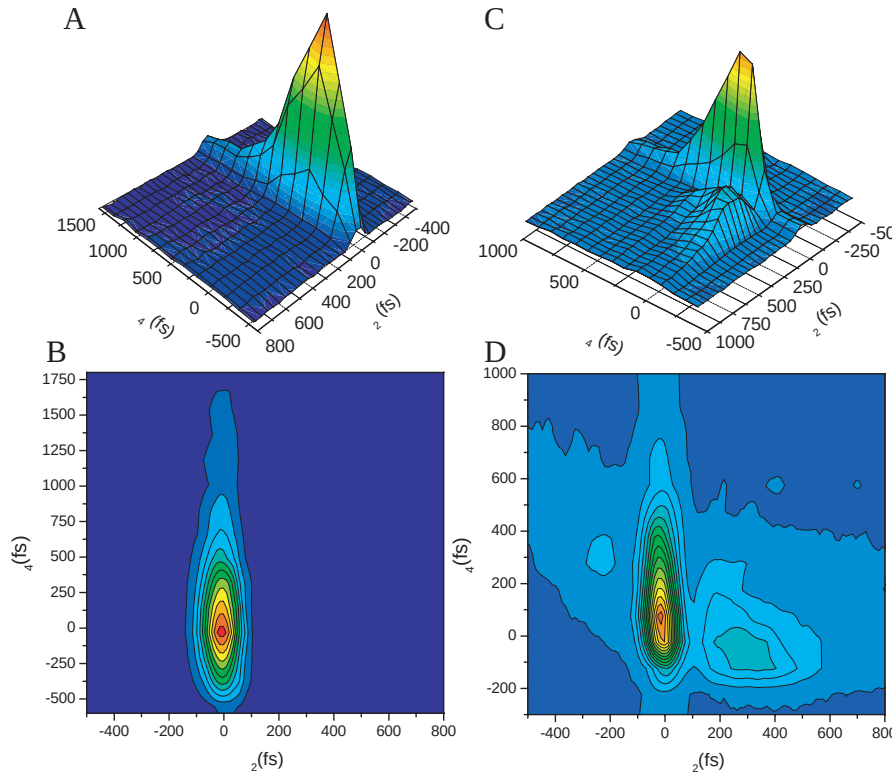

Figure 6. Homodyne detected fifth-order Raman response of liquid CS_2 using two beam geometries with different degrees of phase mismatch for the parallel cascade: (*a*), (*b*) data taken in the crossed-beam geometry; (*c*), (*d*) data taken in the baseball diamond geometry. The τ_4 ridge feature is preserved despite the change in phase matching.

parallel to each other at 0°, while the probe is polarized at 45° and the analyser polarizer that selects the signal polarization is set at −45°. This arrangement was initially used to minimize scattered light from the probe. Since the $R^{(5)}_{121111}$ tensor element is identically zero, the only two tensor elements that could be used to compose this polarization configuration are $R^{(5)}_{221111}$ and $R^{(5)}_{111111}$. The all-parallel tensor element, $R^{(5)}_{111111}$, has the largest magnitude of all the seven tensor elements, and $R^{(5)}_{221111}$is considerably smaller in magnitude by a factor of 20. The two-dimensional response of the all-parallel tensor element was measured using direct (homodyne) detection, but, because of large background probe scattering into the signal direction (i.e. in the absence of any pump fields), the signal-to-noise ratio was superior using the crossed probe and signal polarizations. Although it was not known at the time, the heterodyne detected experiments subsequently showed that the differences between the $R^{(5)}_{111111}$ and $R^{(5)}_{-45,45,1111}$responses to be minimal. As plotted on this contour graph, the all-parallel response is essentially identical to the data shown in figure 6.

The baseball diamond and crossed-beam geometries have identical fifth-order wavevector matching conditions, and the sequential cascaded third-order pathways likewise have the same wavevector matching parameters. The only difference between the geometries is the degree of wavevector mismatch for the parallel

cascaded processes. The most prominent feature of the data shown in figure 6 is the distinctive ridge along the τ_4 axis, with a very fast decay along the diagonal and the τ_2 axis. There is clearly no evidence for vibrational rephasing (or *echo*) in the form of a ridge along the time diagonal ($\tau_2 = \tau_4$). All reported fifth-order Raman measurements preceding this two-colour result, and several subsequent reports, were characterized by extensive signal amplitude along the τ_2 axis—a signature that is not predicted by theory other than cascaded third-order simulations. The lack of the ridge along the pump delay axis, τ_2, was an encouraging sign that the true fifth-order response was responsible for the experimental data.

Following this initial report, homodyne detected results were obtained by Blank *et al.* using the conventional beam-splitter method of generating the required five different beams, and these data were assigned as the direct fifth-order response of liquid CS_2 [42]. In addition to the fully polarized, $R^{(5)}_{111111}$, response, data for a 'magic-angle' configuration, $R^{(5)}_{1111\mathrm{MM}}$, were also reported (where $M = 54.7^\circ$ relative to the other polarizations). It was immediately clear, however, that the results obtained with the two-colour diffractive optic technique and those obtained using the one-colour (800 nm) beam-splitter approach had significant differences. As with the very early fifth-order Raman results, differences in experimental implementation (path length, beam geometries, focusing conditions and wavelengths) made it a challenge to identify the source of the differences of the latest experiments.

As has been mentioned above, one of the truly great benefits of using a diffractive optic for high-order non-linear spectroscopy is the relative ease with which OHD can be employed. Heterodyne detection is straightforward once the relative magnitude of the reference and signal field is appropriately adjusted using a neutral density filter and a half-wave plate in the reference beam—the reference intensity is typically 50–100 times larger than the homodyne-detected signal.

All seven experimentally accessible tensor elements were measured using the two-colour heterodyne detected diffractive optics approach [48], and two particular examples are considered here. The full, two-dimensional response of one tensor element, R_{121211}, is shown in figure 7. These results bear a resemblance to the direct detected data shown above, with the key exception that the nuclear response in the two-dimensional region of the surface (τ_2, $\tau_4 > 0$) is largely composed of a signal that has an opposite phase to the predominant signal feature along the τ_4 axis. For the in-phase data (figures 7 (*a*) and (*b*)), the decays along the τ_2 axis and the diagonal are very rapid, although a clear shoulder is observed for very short probe delays ($\tau_4 < 100$ fs) along the τ_2 axis. This signal is longer than the pulse width of the laser pulses used in the experiment (75 fs full width at half-maximum). The dominant signal feature is, nevertheless, the ridge along the probe delay axis, τ_4.

Following the suggestion of Jansen *et al.*, a new polarization configuration was recently considered where simple theoretical considerations indicate further suppression of unwanted cascaded signals is expected beyond that due to wavevector mismatch and phase selectivity. We have dubbed this experimental configuration the 'Dutch Cross' to denote its origins and crossed pattern. It provides an additional 10^4 contrast against lower-order cascades and serves as an important experimental check on signal purity for any phase matching geometry [49]. The Dutch Cross configuration is denoted $R_{-L-L11LL}$, where $L = 60^\circ$. The 60° angle between successive pairs of pulses ensures that all the intermediate third-order steps result in a nuclear response that is significantly suppressed relative to the polarized tensor element. The Dutch Cross configuration is an excellent check of a particular

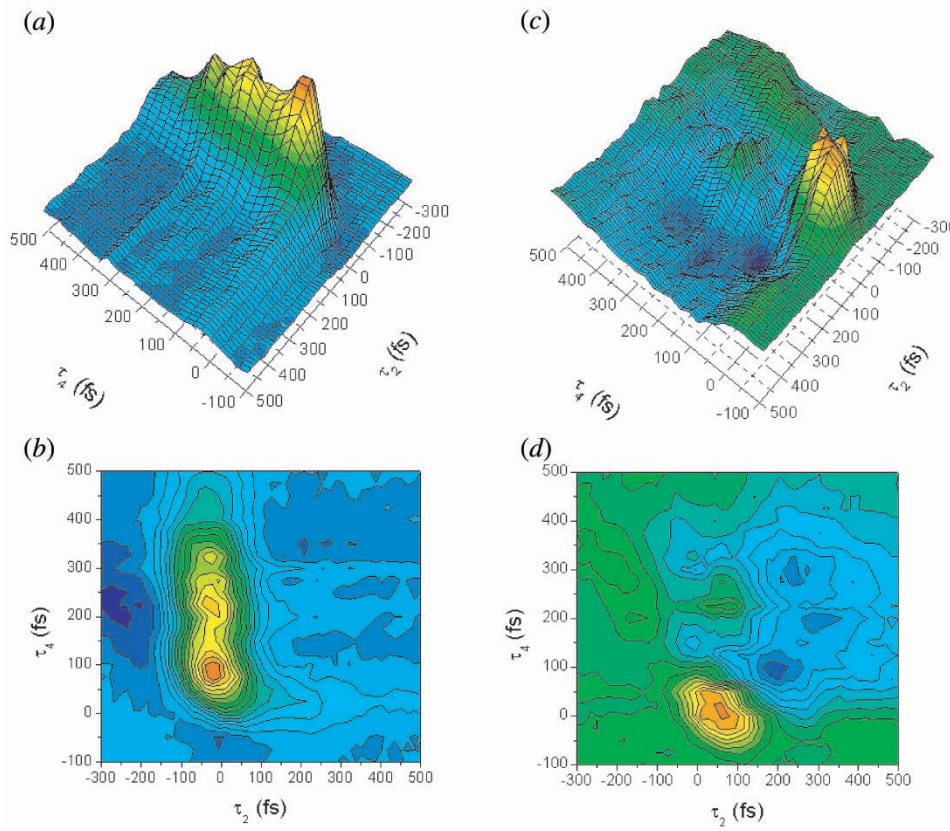

Figure 7. Heterodyne detected fifth-order Raman response of liquid CS_2 for the R_{121211} tensor element: (*a*), (*b*) in-phase component; (*c*), (*d*) data collected at a relative phase of $\pi/2$. The baseball diamond geometry was used to measure these data with a 100 micron pathlength to eliminate cascades. Figures (*a*) and (*b*) reproduced from [46] with permission from Elsevier Science.

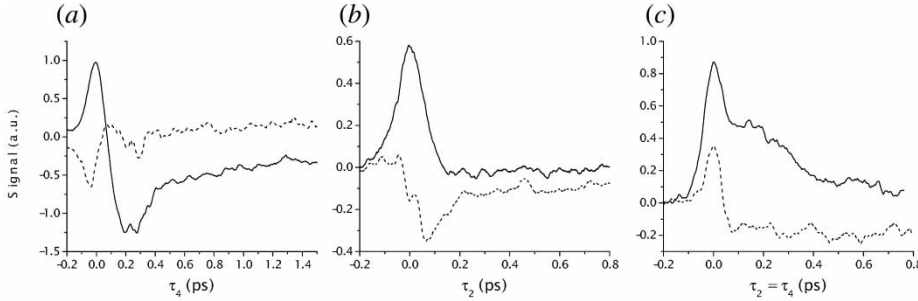

Figure 8. Heterodyne detected fifth-order Raman response of liquid CS_2 for the Dutch Cross configuration. The full curves are the in-phase signals, and the broken curves are the $\pi/2$ shifted signals. (*a*), (*b*) and (*c*) show slices along τ_4, τ_2 and the diagonal respectively. Reproduced from [49] with permission from Elsevier Science.

experimental beam geometry's ability to suppress third-order cascades since there should be no appreciable nuclear signal due to cascades. Figure 8 shows three slices through the two-dimensional surface of the Dutch Cross configuration fifth-order response of liquid CS_2.

The results obtained using the Dutch Cross configuration are particularly interesting owing to the similarities and differences relative to the other tensor elements. As with the majority of measurements of the fifth-order Raman response of liquid CS_2 using the two-colour, heterodyne detection approach, there is an elongated ridge along the τ_4 axis. The data further show that the decay along the τ_2 axis at the probe delay origin, $\tau_4 = 0$, is very rapid. The differences, however, are clearly evident in the pronounced diagonal component that is not observed in other tensor elements. This diagonal feature is, however, not long-lived and falls to zero by 500 fs with a ~320 fs 1/e decay. It is also noteworthy that the nuclear components along the diagonal and τ_4 axis have opposite signs indicating that there is a node in the response. The node along τ_4, which has been predicted in the MD simulations of Saito and Ohmine, has been attributed to anharmonic coupling between translational and rotational degrees of freedom. In the experimental data shown above, however, the node appears to be due to a sign difference between the electronic and nuclear components of the response function rather than a purely nuclear sign change. Since it is not possible to eliminate the electronic hyperpolarizability contribution to the temporal response, the nuclear response node cannot be verified, but it is certainly possible that there is such a node given the sign change between the nuclear contributions along the τ_4 axis and the diagonal. It will be highly informative to consider a model system that can be treated analytically or with reduced numerical complexity (relative to the equilibrium MD simulation), so that any numerical origins for the nodal feature can ruled out. It should be noted, however, that the level of agreement with finite-field as well as equilibrium MD simulations is encouraging. The peak position of the nuclear signal and decay profile are in near quantitative agreement. The strong ridge along τ_4 is also captured. The only difference is the nodal plane bisecting τ_4 in the equilibrium MD simulations which is not observed experimentally in this work; otherwise the complete two-dimensional (2D) spectrum is faithfully reproduced by both MD simulations. In this respect the finite-field MD is closest to the experimental observations but the general features are conserved in both theory and experiment.

The heterodyne detected fifth-order Raman results clearly indicate that there is little rephasing ability in room temperature CS_2. One way to develop an understanding of this evidently 'echoless' echo experiment is to consider the conditions under which an echo can be produced in the first place. In section 2, a harmonic picture was used in order to motivate the MMBO approach for modelling the system–bath dynamics. By revisiting this point, it is possible to illustrate a crucial assumption that is built into the expectations for fifth-order Raman, and one which may, in fact, be untenable. The rephasing response of a single harmonic oscillator is due to a subset of possible field–matter interactions where the non-linear polarizability ($\alpha^{(2)}$) mediated process occurs during the second step [104]. The rephasing process begins with a coherence between the ground and first excited vibrational level, $|0\rangle\langle 1|$ or $|1\rangle\langle 0|$, and this coherence is transferred to a second coherence, $|2\rangle\langle 1|$ or $|1\rangle\langle 2|$, by the second pair of pulses via a two-quantum transition. The probe–signal interaction leaves the system in either $|1\rangle\langle 1|$ or $|2\rangle\langle 2|$ population states. The response of this single oscillator system can be calculated exactly, and the critical term is proportional to $\cos[\omega(\tau_2 - \tau_4)]$, where ω is the frequency of the oscillator [2, 12]. Clearly, this term is a maximum when the two time delays are exactly equal, thus leading to the diagonal ridge, often denoted as an '*echo*'. This echo feature has been observed in models consisting of single oscillators as well

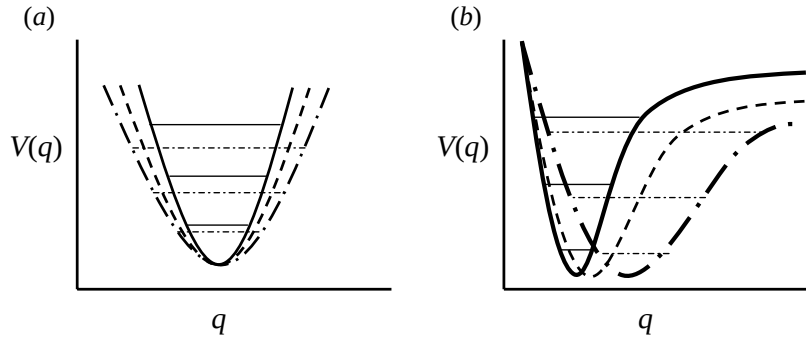

Figure 9. Two models of energy gap fluctuations for (*a*) a harmonic model and (*b*) an anharmonic model. The potential, $V(q)$, is a function of the idealized mode, q, and its time evolution is represented by the different full, broken and chain curves to represent bath fluctuations. For comparison, energy levels are schematically displayed in order to highlight the qualitative differences between the two models regarding evolution to marginally bound configurations.

as multiple Brownian oscillators, and the rephasing survives coupling to a Gaussian bath [83]. The main effect of coupling to a bath is to shift the energy levels, and, depending on the time-correlation function of the frequency modulation, the models can interpolate from homogeneous (rapid modulation) to inhomogeneous (slow modulation) broadening limits [14]. It is worthwhile to mention, however, that the most generally adopted bath model preserves the harmonicity of the system dynamics. In other words, the energy level gaps between all the states of the system are the same at any given time. An example of the type of modulation of the harmonic potential model in this way is shown in figure 9 (*a*). The modulation is essentially the same for all states of the oscillator, and no distinction is made between the low-lying states and the higher energy states. An alternative picture of the modulation due to the coupling to a 'bath' is shown in figure 9 (*b*). In the latter picture, the functional shape of the potential evolves, including the equilibrium position, as well as the anharmonicity. The correlated modulation of the harmonic potential can always be viewed as a simplified picture (or Taylor expanded) version of the more general case shown in figure 9 (*b*) since at any point during the modulation it is possible to refit the true anharmonic potential with a harmonic expansion. The subtle differences between the two system–bath descriptions are not captured by third-order Raman spectroscopy because third-order measurements are determined completely by $\alpha^{(1)}$ processes, and are thus insensitive to anharmonicities. In the fifth-order response, an overtone transition is intimately connected to the induced coherence and is thus much more sensitive to the anharmonic details on the intermolecular potential. The key conceptual point is as follows: in the original work of Tanimura and Mukamel, there is an explicit assumption that the dephasing processes of the $|0\rangle\langle 1|$ or $|1\rangle\langle 0|$, coherence is the same as the overtone-driven $|2\rangle\langle 1|$ or $|1\rangle\langle 2|$ coherence involved in the rephasing step, i.e. the one-quantum and two-quantum transitions have the same correlation with the bath. This assumption was made to make the problem more tractable but needs to be re-examined. The overtone involves motion further from equilibrium fluctuations and may have different couplings to the bath as a result of the increased anharmonicities sampled by this motion. Another way to think about this issue of level-dependent dephasing is that the overtone must be a marginally bound state.

The very use of modes to describe liquids has been questioned as an appropriate basis as even the fundamental mode is strongly damped and rapidly decays into diffusive motions. For example, there is not a large separation in timescale between the inertial motions and subsequent diffusive reorientational decay for CS_2. The overtone should be even more weakly bound and more strongly damped such that level-dependent dephasing should be expected. In such a case, the most rapid dephasing process will dominate the rephasing dynamics and this process would be expected to be derived from the decay in the coherence involving the two-quantum transition. This point can be gleaned from figure 9 in comparing modulation of a harmonic potential and an anharmonic one. In the latter case, the overtone samples a different curvature in the potential so the coupling coefficient to the bath fluctuations should be larger (faster dephasing). Alternatively, the overtone may occur energetically at a point in which it is marginally bound and as the bath evolves, becomes unbounded and clearly overdamped. Both effects lead to level-dependent dephasing. This effect is a bit of serendipity as it is probably the fundamental reason for the high sensitivity of fifth-order Raman to the details of the intermolecular potential. The experiment selectively monitors processes directly correlated to the anharmonic terms in the potential.

As important as the liquid decoherence information is, the fifth-order Raman is found to be even richer in details than that which can be discerned from just the rephasing pathways (diagonal component to the 2D spectrum). To examine more quantitatively the different contributions to the signal source, it is useful to consider model cases. A common prototype for intramolecular motion is the Morse oscillator. For a Morse oscillator coupled to a bath, Tanimura found that the fifth-order response was asymmetric with respect to the two time delays: the decay along the probe delay axis, τ_4, was shown to be slower than the decay along the pump delay axis, τ_2 [87]. The model offers the ability to consider separately differences between harmonic (HO), anharmonic (AH), linear polarizability (LP) and non-linear polarizability (NP). Comparing AH+NP and HO+NP, one sees that the response is 'pulled' toward the τ_4 axis with the anharmonic potential. The difference between AH+LP and AH+NP is that the AH+LP signal reaches a maximum with the two pump pulse pairs time overlapped (i.e. at $\tau_2 = 0$) for any given value of τ_4. In the AH+NP case, however, the signal does not peak until τ_2 reaches a specific non-zero value (in the example used by Tanimura, where the potential was chosen to match the vibrational frequency of the caesium dimer, $\omega_0 = 38.7\,\mathrm{cm}^{-1}$, corresponding to a period of 861 fs, the peak is at roughly 100 fs). The location of the peak—either at $\tau_2 = 0$ or shifted away from the axis—is, in principle, an experimentally measurable difference, and is thus capable of revealing whether the non-linear polarizability is the dominant mechanism. Any electronic/nuclear hyperpolarizability contribution along the τ_4 axis may, however, complicate experimentally discriminating between the nuclear signal that peaks at $\tau_2 = 0$ and one that peaks at $\tau_2 > 0$. In both cases, however, the signature of the anharmonic potential is a ridge-like feature along the τ_4 axis. This feature is observed not only in our experimental results but also in all of the MD simulations of fifth-order response functions performed thus far [6, 15, 21, 22, 92, 97, 98, 133]. Interestingly, the MD simulations of the fifth-order Raman response of liquid xenon show the response to be peaked on the τ_4 axis, while MD simulations for CS_2 show the response to be peaked away from the axis. If the Morse oscillator result is a guide, then the xenon response would be dominated by anharmonicity and linear polarizability, while the CS_2 response is due to

anharmonicity and non-linear polarizability. While this conclusion is tempting, it should be noted that other microscopic mechanisms can lead to the τ_4 ridge, and these will be discussed below.

Tanimura's Morse oscillator model shows that the most basic difference between the response of a single anharmonic mode is characterized by a ridge-like feature along the probe delay axis. As was shown in section 2, in an inhomogeneous mode distribution, introduced either by varying the timescale of the frequency fluctuations or by explicitly including an inhomogeneous distribution, a clear signature of the inhomogeneity is the diagonal rephasing. Tanimura did not examine the case of an inhomogeneously broadened anharmonic oscillator. For a more direct connection to experiment, it would be informative to have a model system where rephasing is a more pronounced effect due to the presence of inhomogeneity while maintaining anharmonic nuclear motion.

In sorting out the possible dynamics that underlie the fifth-order response, it is fortunate that several illuminating MD simulations have been performed in the past two years. In molecular liquids, the dynamics of principal importance to the many-body interactions probed by fifth-order Raman will always be accompanied by a fraction of the signal that is only related to single-molecule orientational dynamics. In order to remove the complexity associated with molecular orientation effects, Ma and Stratt considered the fifth-order response of liquid xenon [15, 92, 97]. The atomic system has the further advantage that a full MD simulation can be performed thus allowing a rigorous comparison between approximate theories and the exact MD response. The first report by Ma and Stratt provided strong evidence that the fifth-order response is particularly sensitive to vibrational anharmonicity [15]. Specifically, the response calculated using instantaneous normal modes (INM) analysis showed a distinct and strong rephasing echo signature along the time diagonal, whereas the MD result completely lacked an echo feature. Since INM is a harmonic theory, the authors concluded that the anharmonicity was the primary difference between the INM and MD treatments. For xenon, the MD response decays very rapidly with increased τ_2, while the response decays much slower along the probe delay axis, τ_4, but is peaked at $\tau_2 = 0$ along that axis. The general features of the data are strikingly similar to those found by Tanimura for the Morse oscillator response [87], adding further support for assigning the disappearance of the echo as well as the τ_4 ridge to anharmonicity. As was shown above, the experimentally determined two-colour heterodyne detected fifth-order data are in particularly good agreement with this form of the response—namely the ridge along the τ_4 axis and the rapid decay along τ_2. The authors explicitly state that the ridge along τ_4 may be seen as an identifying trait of the fifth-order Raman response. Subsequently, Ma and Stratt further refined their description of the microscopic signal origins for the xenon system and, by applying INM analysis with this more sophisticated formulation, found much better agreement between the INM and MD results [92]. The main ingredient in the revised INM treatment was an accounting for anharmonic contributions by incorporating an adiabatic change in the individual INM frequencies. Interestingly, the revised INM treatment also revealed that the non-linear polarizability contribution to the signal was less important than the dynamical anharmonicity.

The comparison of the INM analysis with the MD simulations for an atomic liquid was particularly enlightening and led to a shift in focus toward the importance of anharmonicity. Since there have been no fifth-order Raman experiments

performed on liquid xenon to date, the simulations that are most directly relevant to experiments are those of carbon disulphide. In the last two years, there have been two different approaches used to simulate the fifth-order response of CS_2. The first implementation used a so-called '*finite-field*' method where the fifth-order experiment is simulated by applying electric fields to a simulation box of molecules. Two applied fields are separated by a time delay τ_2 and the net polarization is evaluated a time, τ_4, following the second pulse. By varying τ_2 and τ_4 the full 2D response can be generated. There are some technical issues that must be addressed—particularly regarding potential lower-order contributions to the polarization (although *not* cascaded processes)—and it appears as though these complications can be adequately eliminated.

Jansen *et al*. first applied the finite-field MD approach to liquid CS_2 using a very simple model for the intermolecular interactions through a Lennard-Jones potential [98]. While this model of the dynamics was reasonably successful in reproducing the long-time, diffusive part of the third-order Raman response of CS_2, the simulation failed to capture the short-time ($t < 0.5$ ps) inertial contribution. Since the short-time contribution is dominated by interaction-induced local field effects, the discrepancy between experiment and simulation is unsurprising given the absences of these interactions in the model. This first report did demonstrate, however, that the finite-field MD and conventional MD approaches yielded identical responses using the same molecular potential.

In order to compare simulation with experiment, the model for the dynamics should at least be able to reproduce well-established third-order measurements. There is, however, no guarantee that a model that can faithfully generate the third-order response will be the correct one to describe the far more sensitive fifth-order response owing to the fundamentally central roles of anharmonicity and non-linear polarizability. Jansen *et al*. subsequently incorporated local field effects via dipole-induced dipole (DID) interactions [21]. Using this refined description of the intermolecular interactions, the finite-field MD approach was able to reproduce the third-order response quantitatively. Using the same dynamical model, the fifth-order response for several tensor elements was calculated. The two-dimensional surfaces, $R^{(5)}(\tau_2, \tau_4)$, were only evaluated for relatively short times (200 fs), but they did show a clear absence of any strong rephasing features, and the signals, which generally peaked near τ_2, $\tau_4 \approx 100$ fs, had decayed to nearly half their maximum value by $\tau_2 = \tau_4 = 200$ fs. The rapid decay in the coherence is consistent with the two-colour, heterodyne detected experimental data discussed above.

It is well known from calculations on model Brownian oscillator systems that the fifth-order response is highly sensitive to microscopic details of the molecular interactions. Given this high degree of sensitivity it is conceivable that, for a molecular liquid, the incorporation of local field effects beyond the traditional DID level of interaction may significantly alter the predicted fifth-order response. Indeed, very recent results of Jansen *et al*., where induced multipoles and overlapping electron cloud distributions were added to the description of the intermolecular interactions, show that the fifth-order response becomes dramatically elongated along the τ_4 axis with even faster decays along the τ_2 axis due to these interactions [22]. Multipoles arise from the difference in charge distribution on each atom of the polyatomic molecule, and, while not expected to play a role in atomic liquids, they permit a more general description of the extended nature of real molecules in liquids. On the other hand, electron cloud overlap effects can be

expected to be important even in atoms since the polarizability is ultimately due to the electron density and the spatial distribution of the electrons is naturally altered by the presence of other atoms or molecules at very close range. Electron cloud overlap effects will be more pronounced for highly polarizable species where the number density is such that the exponentially decaying wavefunctions on neighbouring particles can interact. Jansen *et al.* found that there is a measurable contribution due to electron cloud overlap, but it is considerably less significant than the induced multipoles in determining the overall fifth-order response [22]. It is noteworthy that, as the model used for the intermolecular interaction in the treatment of Jansen *et al.* is made more sophisticated, the agreement with experiment improves significantly. It appears theory and experiment are converging.

In addition to the finite-field MD studies, an alternative approach to the computation of the fifth-order response of liquid CS_2 was employed by using an equilibrium MD simulation and evaluation of the classical limit of the response function given in equation (3). A major conceptual advantage of the response function formulation of non-linear spectroscopy is that the classical limit may be readily obtained by making the correspondence between the quantum mechanical commutators and the classical Poisson bracket. The principal computational expense in such a correlation function MD (CFMD) approach is the evaluation of the stability matrix. The simulations of Saito and Ohmine are very similar to those of Jansen *et al.*, further supporting the formal equivalence of the two methods (although each has distinct technical complications) [6]. The main features of the CFMD results are the nuclear peak along the diagonal and subsequent rapid dephasing. These CFMD simulations included only DID interactions. Given the important contribution of induced multipoles as shown by Jansen *et al.*, it will be informative to compare results with the same interactions.

There is one important prediction of the CFMD simulations that is not borne out in the finite-field MD or the two-colour heterodyne experimental results. Saito and Ohmine find nodal features in the fifth-order response due to sign changes of the signal. These nodes were interpreted as arising from coupling between rotational and translational degrees of freedom. Since we do not experimentally observe any evidence for nodes in the nuclear response, it is unclear whether the CFMD results are truly novel predictions or rather due to some unknown numerical sensitivity. Indeed, Saito and Ohmine show calculated two-dimensional surfaces for the three individual terms that constitute the total fifth-order Raman response. While two of these terms have nodes themselves, the predominant topological feature of all three components is a strong ridge along the τ_4 axis (see figure 3 of [6]). The nodal structure in the two-dimensional response may, therefore, be sensitive to the weights given to each of these terms, and may thus be highly sensitive to the precise form of the microscopic interactions. The finite-field MD calculations of Jansen *et al.* do not show these nodes and again it will interesting to compare approaches to determine the source of these differences.

It should be noted that recent single-colour, heterodyne detected fifth-order Raman experiments performed by Kaufman *et al.* have revealed nodes in the spectra [44]. The authors concluded in this work that the heterodyne data are in agreement with the CFMD simulation results based on the common observation of the nodal features. It needs to be pointed out that the heterodyne experiment was performed using the same beam geometry reported earlier, and this particular experimental configuration has been shown to yield results that are most likely dominated by

cascaded third-order signals [49]. In fact, simulated third-order cascades show significantly better agreement with the original homodyne detected data of Kaufman *et al*. than any of the subsequent molecular dynamics simulations. Because of the unfavourable phase difference (168°) [134] between the cascaded third-order signal and the direct fifth-order signal, it is nearly impossible to use heterodyne detection as a method to separate the two contributions unless the magnitude of the direct fifth-order signal itself is larger than the cascaded third-order contribution. (In the original report [44], a 180° phase difference was cited as an approximation. The best estimate based on a calculated cascade response is 168°, which permits a small degree of contrast through the use of phase to discriminate between the cascaded and true fifth-order response.) However, on the basis of the near quantitative degree of agreement over the full 2D spectrum with expected cascaded responses [49], it is most likely that the cascaded third-order signal amplitude is at least an order of magnitude larger than the direct fifth-order signal. In order to isolate a weaker signal from a strong one using heterodyne detection, the phase shift between the two fields should be as close to 90° ($\pi/2$) as possible. The nodes observed by Kaufman *et al*. are therefore probably due to interferences between different cascaded third-order processes and possibly the direct fifth-order response, or interferences involving cascaded third-order processes and electronic/nuclear hyperpolarizability contributions to the fifth-order response. The CFMD simulations (and the finite-field MD simulations) do not treat the electronic/nuclear hyperpolarizability terms at all, and any interference with such terms is entirely unknown. Moreover, the majority of the signal amplitude (at least 90% of the dynamic range) in the data of Kaufman *et al*. is in a large ridge along the τ_2 axis where there is no theoretically predicted signal contribution. This dominant τ_2 ridge is, however, in direct agreement with cascaded third-order simulations. Because of the rather select agreement in certain regions and significantly more pronounced discrepancies between the MD simulations over the full 2D spectrum, and the question surrounding the relative cascade contributions in this experiment, the issue must remain unresolved at present.

Despite the few remaining discrepancies, the convergence of the above experimental data and the theoretical results is rather promising. The single most important lesson from all of this work is that the fifth-order Raman response is extremely sensitive to the intermolecular potential. This finding reinforces that this new form of spectroscopy harbours great potential in giving us our most rigorous testing ground for our understanding of the liquid state. In the case of CS_2, we have now direct insight into the anharmonic coupling and further theoretical analysis of the experimental observations will probably quantify this effect. The rapid decay in the two-time-interval correlation function stands alone as a distinctive feature of the timescales under which liquids evolve. This feature of the liquid dynamics can be discerned in our initial findings that the response decays very rapidly in all directions except the pronounced ridge along the τ_4 axis. The more recent successful implementation of the Dutch Cross polarization configuration confirms that the two-colour heterodyne detected diffractive optic approach has been successful in isolating the direct fifth-order response of CS_2. This work thus represents a significant advance in non-linear optics as a probe of liquids. There were a number of important experimental advances associated with the diffractive optic that made this advance possible. By imposing a severe wavevector mismatch for the third-order cascaded processes, the amplitudes of the competing signal components are dramatically reduced. By taking care to ensure a favourable near-$\pi/2$ phase shift

between any residual cascades and the direct fifth-order signal, it was possible to take advantage of the linearization, amplification and phase contrast benefits of optical heterodyne detection. Heterodyne detection itself was made possible in large part because of the diffractive optic approach to generating the required six interacting laser beams with very high relative phase stability. It should also be mentioned that a preliminary report by Kaufmann *et al.* using the Dutch Cross configuration and a reworked phase matching geometry similar to ours is now virtually identical to our findings [135] with respect to the strong ridge along τ_4, fast dephasing and, most importantly, the absence of signal along τ_2 confirming the removal of cascades. Experiment and theory are converging on all fronts.

It appears that the challenge to determine the electronically non-resonant fifth-order nuclear response of liquids as a direct probe of the two-time-interval correlation function has been met. The experiment was originally envisioned as a means to separate homogeneous and inhomogeneous contributions to the low-frequency intermolecular spectrum of liquids. The experiment has shown itself to be far richer in details; both in understanding the liquid state and also in the understanding of higher-order non-linear spectroscopies. Further refinements in both theory and experiment will probably reveal the relative contributions of various important physical parameters such as anharmonicity, non-linear polarizability, interaction-induced local field effects and rotational–translational couplings to give perhaps the most detailed description of a liquid possible from experimentally derived parameters.

5. Future directions

In all fields of spectroscopy, it has become increasingly clear that multidimensional techniques are required in order to access fundamentally new information [19, 25]. While it is always possible to imagine shorter-duration, wider-bandwidth laser pulses and ultrashort pulses in spectral regions that have been traditionally difficult to access, the limitations of one-dimensional measurements remain. Because of significant advances in femtosecond amplifier technology and non-linear parametric generation, it is now possible to conceive of coherent, multicolour even *multiprocess* interactions combining various previously distinct techniques in order to access new dynamical correlations. Indeed, one such approach that combines IR and Raman interactions has already proven capable of opening new windows into intermolecular dynamics [24, 136]. Recent progress towards isolating the true fifth-order Raman response of a liquid has already helped to refine our picture of microscopic liquid dynamics while clarifying and focusing the vocabulary used to discuss condensed phase systems beyond simple harmonic descriptions. In order to establish fifth-order Raman as a general methodology, however, other liquids must be shown to be amenable to such a high-order non-resonant probe. The overdamped, rapidly decaying response of CS_2 should not be taken as universal. More structured liquids such as strongly associated hydrogen-bonded liquids, so important to understanding biological systems, should show longer-range correlations. There are several such avenues that are ripe for exploration in the coming years, and a few of these are discussed below.

The pinnacle of liquids is water. The many peculiar and spectacular properties of water are directly related to the very strong hydrogen bonding interactions long known to produce a highly structured (although transient) network of molecules.

From a biological perspective, hydrogen bonds are not only responsible for the interactions in water, but are also the principal glue holding together the two strands of DNA, while playing key roles in intraprotein as well as protein–protein interactions. Indeed, a full description of pure liquid water is only biochemically important insofar as it represents a baseline against which to compare the far more important electrolytic solutions of buffered media where the structure and dynamics may be significantly different from the neat liquid. There is therefore ample motivation to apply fifth-order Raman spectroscopy to the study of water and aqueous solutions.

Unfortunately, the Raman polarizability of water is considerably lower than that of CS_2, and CS_2 already requires a state-of-the-art laser system in order to produce pulses with sufficient bandwidth and energy to observe a fifth-order Raman signal. Extending the present experimental approach to water, therefore, will require a paradigm shift (or at least a *semi*revolution) in amplified ultrafast laser sources. Naturally, work is currently in progress to exceed the current limitations of conventional regenerative and multipass schemes for generating high repetition rate millijoule near-IR pulses with sub 10 fs pulse durations, but such progress is necessarily slow. Nevertheless, once such next-generation laser technology is eventually realized, the multicolour, heterodyne detected, diffractive optics based strategy will be very well suited to the study of new systems. The effort already expended to identify experimental complications will significantly accelerate the interpretation of new results since we now have a straightforward protocol by which to ensure the integrity of fifth-order Raman measurements.

In the meantime, it is also possible to use fifth-order Raman spectroscopy to investigate the multidimensional spectra of lower-frequency intramolecular modes. There is a richness of information contained in motions with frequencies below $1000\,cm^{-1}$—commonly known as 'fingerprint' regions—and, since these modes may have less complicated dynamics than the very-low-frequency liquid motions described here (i.e. differences between fundamental and overtone dephasing), modelling the dynamics may prove to be far simpler while still being able to probe interesting mode–mode couplings. Fifth-order Raman offers a unique opportunity to measure directly the coupling between low-frequency intramolecular modes and the bath. There are also some liquids, such as CCl_4, with intramolecular modes that are within the spectral bandwidth of currently available laser pulses [41]. Now that we have a clearer prescription for avoiding low-order artifacts, measurements of intramolecular modes can certainly be revisited. The relatively long dephasing time (typically $\sim$1–3 ps) of intramolecular modes further reduces the difficulty of performing coherent multidimensional Raman spectroscopy and allows for the possibility of separating population decay, level-dependent dephasing and anharmonicity contributions where the timescales may be separated.

In addition to conventional studies of liquids, it would also be interesting to investigate the fifth-order response of glassy systems, where, because of distributions of relaxation pathways, the dynamics are characterized by non-exponential decays. In structural glasses, the differences in relaxation rates are due to inhomogeneously distributed distinct local structures and are thus perfect candidate systems in which to observe a clear vibrational echo. Changes in the rephasing character as the system is brought through the glass transition would help to address key questions about the presence or absence of the echo rephasing pathways with respect to competing influences of level-dependent dephasing, mode mixing

through polarizability and vibrational anharmonicity. As in the above discussion, the challenge facing glass studies will be to find a material with a large fifth-order response.

Another obvious tract will be to explore supercooled and supercritical liquids. The latter may prove to be extremely interesting as the liquid potential under these conditions is in a rarified state and anharmonic contributions should be manifest in the fifth-order Raman signal, as predicted on theoretical grounds [95]. At present, it is difficult to predict the magnitude of the fifth-order response on the basis of readily available parameters such as dielectric constant and Raman polarizability (i.e. linear polarizability). Once certain classes of liquids are found amenable to fifth-order Raman, it will be very interesting to subject these systems to pressure, temperature studies that place that liquid along various points in the phase diagram and to supercritical conditions to evaluate the intermolecular potentials rigorously.

In addition to promising experimental advances, there are also several theoretical developments that will prove invaluable in interpreting fifth-order Raman spectroscopy of new liquids. Besides the two MD approaches discussed here, there are also analytical theories that can help to bring physical insight to the often mysterious results of simulation. That is to say, the results of exact MD simulations give correct answers, but typically at the expense of physical meaning. New treatments of liquid dynamics using molecular hydrodynamic theories have been shown to capture certain elements of the fifth-order response of liquid xenon (by comparison with the MD simulation of Ma and Stratt [15, 97]). In particular the work both of Denny and Reichman [16, 94, 95] and of Cao *et al.* [96] predicts an echoless response with an asymmetric response similar to that found in the exact MD simulation, and, as stated above, qualitatively similar to our experimental results for CS_2. Molecular hydrodynamic theories require relatively straightforward input in order to compute the response functions and thus represent a convenient approach that should be readily adapted to new liquid systems without requiring an MD simulation for validation, although there are always approximations whose appropriateness must be verified. The joint application of INM (both with and without anharmonicity and non-linear polarizability), hydrodynamic theory and MD simulations, in conjunction with more traditional Brownian oscillator models, will probably form a general basis for interpreting complicated high-order response functions. Since one of the chief *goals* of experimental fifth-order spectroscopy is to further refine liquid potential functions, it seems only sensible to assume that our current understanding of liquid potentials is incomplete, and the main opportunity to learn about liquids is by mending discrepancies between theoretical results and experimental data. A change to this new direction of information flow should be more appealing now that the experimental difficulties of fifth-order Raman spectroscopy have been identified and in certain cases eliminated. It is, therefore, decreasingly necessary to rely on theoretical 'checks' of the measured data. In fact, this new trend has been realized in the recent work of Jansen *et al.* where the strong asymmetry in the heterodyne detected data, and the ridge along the τ_4 axis, was able to motivate (or at least be explained by) a consideration of higher-order local field effects [22, 133].

References

[1] Titus, T. N., Kieffer, H. H., and Christensen, P. R., 2003, *Science*, **299**, 1048–1051.
[2] Tanimura, Y., and Mukamel, S., 1993, *J. Chem. Phys.*, **99**, 9496–9511.

[3] Mukamel, S., 2000, *Annu. Rev. Phys. Chem.*, **51**, 691–729.
[4] Mukamel, S., Piryatinski, A., and Chernyak, V., 1999, *Acc. Chem. Res.*, **32**, 145–154.
[5] Saito, S., and Ohmine, I., 1998, *J. Chem. Phys.*, **108**, 240–251.
[6] Saito, S., and Ohmine, I., 2002, *Phys. Rev. Lett.*, **88**, 207401.
[7] Cho, M. H., Okumura, K., and Tanimura, Y., 1998, *J. Chem. Phys.*, **108**, 1326–1334.
[8] Okumura, K., and Tanimura, Y., 1997, *J. Chem. Phys.*, **107**, 2267–2283.
[9] Steffen, T., and Tanimura, Y., 2000, *J. Phys. Soc. Jpn.*, **69**, 3115–3132.
[10] Hahn, S., Park, K., and Cho, M., 1999, *J. Chem. Phys.*, **111**, 4121–4130.
[11] Cho, M. H., 2000, *J. Chem. Phys.*, **112**, 9978–9985.
[12] Steffen, T., Fourkas, J. T., and Duppen, K., 1996, *J. Chem. Phys.*, **105**, 7364–7382.
[13] Steffen, T., and Duppen, K., 1998, *Chem. Phys. Lett.*, **290**, 229–236.
[14] Steffen, T., and Duppen, K., 1998, *Chem. Phys.*, **233**, 267–285.
[15] Ma, A., and Stratt, R. M., 2000, *Phys. Rev. Lett.*, **85**, 1004–1007.
[16] Denny, R. A., and Reichman, D. R., 2001, *Phys. Rev. E*, **63**, 065101.
[17] Cao, J. S., Yang, S. L., and Wu, J. L., 2002, *J. Chem. Phys.*, **116**, 3760–3776.
[18] Okumura, K., Tokmakoff, A., and Tanimura, Y., 1999, *J. Chem. Phys.*, **111**, 492–503.
[19] Fourkas, J. T. 2002, *Annu. Rev. Phys. Chem.*, **53**, 17–40.
[20] Murry, R. L., Fourkas, J. T., and Keyes, T., 1998, *J. Chem. Phys.*, **109**, 7913–7922.
[21] Jansen, T. l. C., Snijders, J. G., and Duppen, K., 2001, *J. Chem. Phys.*, **114**, 10910–10921.
[22] Jansen, T. l. C., Duppen, K., and Snijders, J. G., 2003, *Phys. Rev. B*, **67**, 134206.
[23] Vandenbout, D., Muller, L. J., and Berg, M., 1991, *Phys. Rev. Lett.*, **67**, 3700–3703.
[24] Zhao, W., and Wright, J. C. 2000, *Phys. Rev. Lett.*, **84**, 1411–1414.
[25] Wright, J. C., 2002, *Int. Rev. Phys. Chem.*, **21**, 185–255.
[26] Asplund, M. C., Zanni, M. T., and Hochstrasser, R. M., 2000, *Proc. Natl. Acad. Sci. USA*, **97**, 8219–8224.
[27] Zanni, M. T., Asplund, M. C., and Hochstrasser, R. M., 2001, *J. Chem. Phys.*, **114**, 4579–4590.
[28] Ge, N. H., and Hochstrasser, R. M., 2002, *PhysChemComm*, **3**, 17–26.
[29] Stenger, J., Madsen, D., Hamm, P., Nibbering, E. T. J., and Elsaesser, T., 2002, *J. Phys. Chem. A*, **106**, 2341–2350.
[30] Woutersen, S., Mu, Y., Stock, G., and Hamm, P., 2001, *Chem. Phys.*, **266**, 137–147.
[31] Palese, S., Buontempo, J. T., Schilling, L., Lotshaw, W. T., Tanimura, Y., Mukamel, S., and Miller, R. J. D., 1994, *J. Phys. Chem.*, **98**, 12466–12470.
[32] Tominaga, K., and Yoshihara, K., 1995, *Phys. Rev. Lett.*, **74**, 3061–3064.
[33] Tominaga, K., Keogh, G. P., Naitoh, Y., and Yoshihara, K., 1995, *J. Raman Spectrosc.*, **26**, 495–501.
[34] Tominaga, K., and Yoshihara, K., 1996, *J. Chem. Phys.*, **104**, 1159–1162.
[35] Tominaga, K., and Yoshihara, K., 1996, *J. Chem. Phys.*, **104**, 4419–4426.
[36] Steffen, T., and Duppen, K., 1996, *Phys. Rev. Lett.*, **76**, 1224–1227.
[37] Steffen, T., and Duppen, K., 1997, *J. Chem. Phys.*, **106**, 3854–3864.
[38] Steffen, T., Meinders, N. A. C. M., and Duppen, K., 1998, *J. Phys. Chem. A*, **102**, 4213–4221.
[39] Tokmakoff, A., and Fleming, G. R., 1997, *J. Chem. Phys.*, **106**, 2569–2582.
[40] Tokmakoff, A., Lang, M. J., Larsen, D. S., and Fleming, G. R., 1997, *Chem. Phys. Lett.*, **272**, 48–54.
[41] Tokmakoff, A., Lang, M. J., Larsen, D. S., Fleming, G. R., Chernyak, V., and Mukamel, S., 1997, *Phys. Rev. Lett.*, **79**, 2702–2705.
[42] Blank, D. A., Kaufman, L. J., and Fleming, G. R., 2000, *J. Chem. Phys.*, **113**, 771–778.
[43] Kaufman, L. J., Blank, D. A., and Fleming, G. R., 2001, *J. Chem. Phys.*, **114**, 2312–2331.
[44] Kaufman, L. J., Heo, J. Y., Ziegler, L. D., and Fleming, G. R., 2002, *Phys. Rev. Lett.*, **88**, 207402.
[45] Astinov, V., Kubarych, K. J., Milne, C. J., and Miller, R. J. D., 2000, *Opt. Lett.*, **25**, 853–855.

[46] Astinov, V., Kubarych, K. J., Milne, C. J., and Miller, R. J. D., 2000, *Chem. Phys. Lett.*, **327**, 334–342.
[47] Kubarych, K. J., Milne, C. J., Lin, S., and Miller, R. J. D., 2002, *Appl. Phys. B*, **74**, S107–S112.
[48] Kubarych, K. J., Milne, C. J., Lin, S., Astinov, V., and Miller, R. J. D., 2002, *J. Chem. Phys.*, **116**, 2016–2042.
[49] Kubarych, K. J., Milne, C. J., and Miller, R. J. D., 2003, *Chem. Phys. Lett.*, **369**, 635–642.
[50] Hahn, E. L., 1950, *Phys. Rev.*, **80**, 580–594.
[51] Weiner, A. M., De Silvestri, S., and Ippen, E. P., 1985, *J. Opt. Soc. Am. B*, **2**, 654–662.
[52] Cho, M. H., Scherer, N. F., Fleming, G. R., and Mukamel, S., 1992, *J. Chem. Phys.*, **96**, 5618–5629.
[53] Leitenstorfer, A., Lohner, A., Rick, K., Leisching, P., Elsaesser, T., Kuhn, T., Rossi, F., Stolz, W., and Ploog, K., 1994, *Phys. Rev. B*, **49**, 16372–16380.
[54] de Boeij, W. P., Pshenichnikov, M. S., and Wiersma, D. A., 1998, *Annu. Rev. Phys. Chem.*, **49**, 99–123.
[55] de Boeij, W. P., Pshenichnikov, M. S., and Wiersma, D. A., 1996, *J. Phys. Chem.*, **100**, 11806–11823.
[56] Jimenez, R., van Mourik, F., Yu, J. Y., and Fleming, G. R., 1997, *J. Phys. Chem. B*, **101**, 7350–7359.
[57] Pshenichnikov, M. S., Duppen, K., and Wiersma, D. A., 1995, *Phys. Rev. Lett.*, **74**, 674–677.
[58] Groot, M.-L., Yu, J. Y., Agarwal, R., Norris, J. R., and Fleming, G. R., 1998, *J. Phys. Chem. B*, **102**, 5923–5931.
[59] Kalpouzos, C., Lotshaw, W. T., McMorrow, D., and Kenney-Wallace, G. A., 1987, *J. Phys. Chem.*, **91**, 2028–2030.
[60] Palese, S., Schilling, L., Miller, R. J. D., Staver, P. R., and Lotshaw, W. T., 1994, *J. Phys. Chem.*, **98**, 6308–6316.
[61] Castner, E. W., and Maroncelli, M., 1998, *J. Mol. Liq.*, **77**, 1–36.
[62] Deeg, F. W., and Fayer, M. D., 1990, *J. Mol. Liq.*, **45**, 19–24.
[63] Smith, N. A., and Meech, S. R., 2002, *Int. Rev. Phys. Chem.*, **21**, 75–100.
[64] Fleming, G. R., and Cho, M. H., 1996, *Annu. Rev. Phys. Chem.*, **47**, 109–134.
[65] Passino, S. A., Nagasawa, Y., and Fleming, G. R., 1997, *J. Chem. Phys.*, **107**, 6094–6108.
[66] Hybl, J. D., Yu, A., Farrow, D. A., and Jonas, D. M., 2002, *J. Phys. Chem. A*, **106**, 7651–7654.
[67] Jimenez, R., Case, D. A., and Romesberg, F. E., 2002, *J. Phys. Chem. B*, **106**, 1090–1103.
[68] Lotshaw, W. T., Mcmorrow, D., Kalpouzos, C., and Kenney-Wallace, G. A., 1987, *Chem. Phys. Lett.*, **136**, 323–328.
[69] Deeg, F. W., Stankus, J. J., Greenfield, S. R., Newell, V. J., and Fayer, M. D., 1989, *J. Chem. Phys.*, **90**, 6893–6902.
[70] Wynne, K., Galli, C., and Hochstrasser, R. M., 1992, *Chem. Phys. Lett.*, **193**, 17–22.
[71] Chang, Y. J., and Castner, E. W., 1996, *J. Phys. Chem.*, **100**, 3330–3343.
[72] Kohles, N., and Laubereau, A., 1987, *Chem. Phys. Lett.*, **138**, 365–370.
[73] Aechtner, P., and Laubereau, A., 1991, *Chem. Phys.*, **149**, 419–425.
[74] Lindenberger, F., Rauscher, C., Purucker, H. G., and Laubereau, A., 1995, *J. Raman Spectrosc.*, **26**, 835–840.
[75] Hattori, T., Terasaki, A., and Kobayashi, T., 1987, *Phys. Rev. A*, **35**, 715–724.
[76] Nibbering, E. T. J., Wiersma, D. A., and Duppen, K., 1992, *Phys. Rev. Lett.*, **68**, 514–517.
[77] McMorrow, D., Lotshaw, W. T., and Ga, K.-W., 1988, *Chem. Phys. Lett.*, **145**, 309–314.
[78] Lotshaw, W. T., McMorrow, D., Thantu, N., Melinger, J. S., and Kitchenham, R., 1995, *J. Raman Spectrosc.*, **26**, 571–583.

[79] Farrer, R. A., Loughnane, B. J., and Fourkas, J. T., 1997, *J. Phys. Chem. A*, **101**, 4005–4010.
[80] Geirnaert, M. L., Gale, G. M., and Flytzanis, C., 1984, *Phys. Rev. Lett.*, **52**, 815–818.
[81] Loring, R. F., and Mukamel, S., 1985, *J. Chem. Phys.*, **83**, 2116–2128.
[82] Tokmakoff, A., 1996, *J. Chem. Phys.*, **105**, 1–12.
[83] Khidekel, V., Chernyak, V., and Mukamel, S., 1996, *J. Chem. Phys.*, **105**, 8543–8555.
[84] Okumura, K., and Tanimura, Y., 1997, *Chem. Phys. Lett.*, **278**, 175–183.
[85] Tanimura, Y., and Okumura, K., 1997, *J. Chem. Phys.*, **106**, 2078–2095.
[86] Okumura, K., and Tanimura, Y., 1997, *J. Chem. Phys.*, **106**, 1687–1698.
[87] Tanimura, Y., 1998, *Chem. Phys.*, **233**, 217–229.
[88] Tominaga, K., and Yoshihara, K., 1998, *J. Phys. Chem. A*, **102**, 4222–4228.
[89] Kirkwood, J. C., Albrecht, A. C., and Ulness, D. J., 1999, *J. Chem. Phys.*, **111**, 253–271.
[90] Kirkwood, J. C., and Albrecht, A. C., 2000, *J. Raman Spectrosc.*, **31**, 107–124.
[91] Keyes, T., and Fourkas, J. T., 2000, *J. Chem. Phys.*, **112**, 287–293.
[92] Ma, A., and Stratt, R. M., 2002, *J. Chem. Phys.*, **116**, 4972–4984.
[93] Tanimura, Y., and Steffen, T., 2000, *J. Phys. Soc. Jpn.*, **69**, 4095–4106.
[94] Denny, R. A., and Reichman, D. R., 2002, *J. Chem. Phys.*, **116**, 1979–1986.
[95] Denny, R. A., and Reichman, D. R., 2002, *J. Chem. Phys.*, **116**, 1987–1994.
[96] Cao, J. S., Wu, J. L., and Yang, S. L., 2002, *J. Chem. Phys.*, **116**, 3739–3759.
[97] Ma, A., and Stratt, R. M., 2002, *J. Chem. Phys.*, **116**, 4962–4971.
[98] Jansen, T. l. C., Snijders, J. G., and Duppen, K., 2000, *J. Chem. Phys.*, **113**, 307–311.
[99] Jansen, T. l. C., Swart, M., Jensen, L., Van Duijnen, P. T., Snijders, J. G., and Duppen, K., 2002, *J. Chem. Phys*, **116**, 3277–3285.
[100] Jansen, T. l. C., Pugzlys, A., Cringus, G. D., Snijders, J. G., and Duppen, K., 2002, *J. Chem. Phys.*, **116**, 9383–9391.
[101] Yee, T. K., and Gustafson, T. K., 1978, *Phys. Rev. A*, **18**, 1597–1617.
[102] Mukamel, S., 1995, *Principles of Nonlinear Optical Spectroscopy* (New York: Oxford University Press).
[103] Bloembergen, N., 1991, *Nonlinear Optics* (Redwood City, CA: Addison-Wesley).
[104] Murry, R. L., and Fourkas, J. T., 1997, *J. Chem. Phys.*, **107**, 9726–9740.
[105] Hura, G., Sorenson, J. M., Glaeser, R. M., and Head-Gordon, T., 2000, *J. Chem. Phys.*, **113**, 9140–9148.
[106] Matsumoto, M., Saito, S., and Ohmine, I., 2002, *Nature*, **416**, 409–413.
[107] Stratt, R. M., 1995, *Acc. Chem. Res.*, **28**, 201–207.
[108] Goodyear, G., and Stratt, R. M., 1996, *J. Chem. Phys.*, **105**, 10050–10071.
[109] Ladanyi, B. M., and Stratt, R. M., 1998, *J. Phys. Chem. A*, **102**, 1068–1082.
[110] Ivanecky, J. E., and Wright, J. C., 1993, *Chem. Phys. Lett.*, **206**, 437–444.
[111] Ulness, D. J., Kirkwood, J. C., and Albrecht, A. C., 1998, *J. Chem. Phys.*, **108**, 3897–3902.
[112] Blank, D. A., Kaufman, L. J., and Fleming, G. R., 1999, *J. Chem. Phys.*, **111**, 3105–3114.
[113] Tominaga, K., Keogh, G. P., and Yoshihara, K., 1995, *J. Mol. Liq.*, **65–66**, 389–392.
[114] Tominaga, K., and Yoshihara, K., 1996, *Phys. Rev. Lett.*, **76**, 987–990.
[115] Tominaga, K., and Yoshihara, K., 1997, *Phys. Rev. A*, **55**, 831–834.
[116] Tominaga, K., 1999, *Laser Chem.*, **19**, 117–122.
[117] Tominaga, K., and Maekawa, H., 2000, *J. Lumin.*, **87–89**, 101–104.
[118] Tominaga, K., and Yoshihara, K., 2000, *J. Chin. Chem. Soc.*, **47**, 631–635.
[119] Steffen, T., Nakashima, S., and Duppen, K., 1999, *Laser Chem.*, **19**, 91–96.
[120] Tokmakoff, A., Lang, M. J., Jordanides, X. J., and Fleming, G. R., 1998, *Chem. Phys.*, **233**, 231–242.
[121] Dadusc, G., Goodno, G. D., Chiu, H. L., Ogilvie, J., and Miller, R. J. D., 1998, *Isr. J. Chem.*, **38**, 191–206.

[122] Goodno, G. D., Dadusc, G., and Miller, R. J. D., 1998, *J. Opt. Soc. Am. B*, **15**, 1791–1794.
[123] Goodno, G. D., and Miller, R. J. D., 1999, *J. Phys. Chem. A*, **103**, 10619–10629.
[124] Goodno, G. D., Astinov, V., and Miller, R. J. D., 1999, *J. Phys. Chem. B*, **103**, 603–607.
[125] Dadusc, G., Ogilvie, J. P., Schulenberg, P., Marvet, U., and Miller, R. J. D., 2001, *Proc. Natl. Acad. Sci. USA*, **98**, 6110–6115.
[126] Eesley, G. L., Levenson, M. D., and Song, J. J., 1977, *IEEE J. Quantum Electron.*, **13**, D31–D32.
[127] Chang, Y. J., and Castner, E. W., 1993, *J. Chem. Phys.*, **99**, 113–125.
[128] Golonzka, O., Demirdoven, N., Khalil, M., and Tokmakoff, A., 2000, *J. Chem. Phys.*, **113**, 9893–9896.
[129] Gallagher, S. M., Albrecht, A. W., Hybl, T. D., Landin, B. L., Rajaram, B., and Jonas, D. M., 1998, *J. Opt. Soc. Am. B*, **15**, 2338–2345.
[130] Hybl, J. D., Faeder, S. M. G., Albrecht, A. W., Tolbert, C. A., Green, D. C., and Jonas, D. M., 2000, *J. Lumin.*, **87–89**, 126–129.
[131] Bonvalet, A., Nagle, J., Berger, V., Migus, A., Martin, J. L., and Joffre, M., 1996, *Phys. Rev. Lett.*, **76**, 4392–4395.
[132] Berne, B. J., and Pecora, R., 1976, D*ynamic Light Scattering with Applications to Chemistry, Biology, and Physics* (New York: Dover).
[133] Jansen, T. I. C., 2002, PhD thesis, Proefschrift Rijksuniversiteit Groningen, Groningen.
[134] Kaufman, L., and Fleming, G. R., 2001, private communication.
[135] Kaufman, L. J., Saito, S., Ziegler, L. D., Ohmine, I., and Fleming, G. R., 2003, *Ultrafast Phenomena XIII*, edited by R. J. D. Miller, M. M. Murnane, N. F. Scherer, and A. M. Weiner (Berlin: Springer), p. 554.
[136] Zhao, W., Murdoch, K. M., Condon, N. J., Besemann, D. M., Meyer, K. A., Chen, P. C., Hamilton, J. P., Zilian, A., Labuda, M. J., Thompson, D. E., Carlson, R. J., Hurst, G. B., Riebe, M. T., Steehler, J. K., and Wright, J. C., 2000, *J. Lumin.*, **87–89**, 90–95.